THE ASTROPHYSICAL JOURNAL, 225:815–842, 1978 November 1

THE GAS DISTRIBUTION IN THE CENTRAL REGION OF THE GALAXY. I. ATOMIC HYDROGEN

W. B. BURTON AND H. S. LISZT
National Radio Astronomy Observatory,* Green Bank, West Virginia
Received 1978 February 3; accepted 1978 May 8

ABSTRACT

We describe a simple model of the distribution and kinematics of gas within 1.5 pc of the galactic center; the model refers to all such gas, whether at apparently permitted or anomalous velocities. The inner-Galaxy material is confined in a layer of scale height 0.1 kpc to a disk of 3 kpc diameter, which is tilted 22° with respect to the plane $b = 0°$ and 78° with respect to the plane of the sky. Within this disk the kinematics involve rotation and expansion of approximately equal magnitude, $\sim 170 \text{ km s}^{-1}$. Detailed specification of the model parameters arises from comparison of synthetic 21 cm emission profiles with a new set of high-sensitivity H I data. The resultant model accounts in a coherent way for many observed spectral features which were previously studied separately and variously identified with bars, spiral arms, or isolated ejecta. In particular the model subsumes the individual features E, J2, J4, J5, VII, X, and XII which were previously considered as evidence of recurring, collimated ejections from the galactic nucleus. The model accounts for the "rotating nuclear disk" feature, which has been the principal source of the inner-Galaxy gravitational field, and subsumes several other extended spectral features (such as III, the "connecting arm") at velocities which are permitted by pure rotation. The H I mass of the disk is $1 \times 10^7 M_\odot$, and the expansion flux across its outer boundary is $4 M_\odot \text{ yr}^{-1}$.

We see no evidence of important density enhancements or kinematic perturbations associated with particular observed spectral features, and see no evidence of anisotropic ejection from the nucleus. The complete axial symmetry shared by all parameters of our synthesis suggests that a steady state prevails. The large-scale consequences of the fundamental inner-Galaxy distribution depends on the total mass involved. Lacking a dynamical foundation, the principal use of the phenomenological model is the constraint of other interpretations of the inner-Galaxy gas.

Subject headings: galaxies: internal motions — galaxies: Milky Way — galaxies: nuclei — galaxies: structure — radio sources: 21 cm radiation

I. PERSPECTIVE

Earlier papers interpreting the wide variety of anomalous-velocity, nonplanar phenomena observed in H I toward the central region of the Galaxy have considered them as ejecta produced by violent activity in the galactic nucleus (see the review by Oort 1977). To account for the many apparently isolated H I spectral features, a high number of discrete and highly collimated events have been invoked, with the epoch and imparted initial velocity of each being tailored in accordance with the individual feature's observed properties. Such explanations are unsatisfying because of the number of unrelated events which they require and because they address directly neither the nature of the ejection mechanism nor the focusing. Also puzzling is the general lack of disruption of the nuclear region gas, which remains predominantly neutral and quite conducive to molecule formation, and confinement of the anomalous-velocity features to a range of velocities $|v| < 280 \text{ km s}^{-1}$.

We offer in this paper an alternative, phenomenological model which accounts in a simple and coherent manner for many of the anomalous phenomena observed toward the galactic nucleus. The gas within 1.5 kpc of the galactic center apparently resides in a rotating and expanding disk which is tilted with respect to the plane $b = 0°$ and to the plane of the sky; within this disk, the matter is well behaved and evidently in a relaxed state. It is the plane of this disk, not the plane $b = 0°$, which is fundamental to the gas distribution in the inner Galaxy, and it is the material in this disk which presumably should provide the inner-Galaxy rotation curve. Although it has been recognized for some time that forbidden-velocity material occurs preferentially in the two opposed quadrants $l > 0°$, $b < 0°$ and $l < 0°$, $b > 0°$ (e.g., Kerr 1967; van der Kruit 1970; Cohen 1975), this has usually been taken as evidence only of a favored collimation axis for the violent events discussed above. Here we stress that essentially *all* of the inner-Galaxy material within 1.5 kpc of the center—whether at seemingly allowed or forbidden velocities—lies in an inclined plane. Furthermore, an axisymmetric model, in which velocity varies smoothly and density varies only with distance from the mean plane of the disk, is capable of synthesizing a wide variety

* Operated by Associated Universities, Inc., under contract with the National Science Foundation.

of "discrete" features. We see no evidence for density enhancements or kinematic perturbations which would indicate either the violent ejection of compact features from the galactic nucleus or the existence of arc-like entities close to it. We show that the appearance of apparently isolated and anomalous spectral features is a consequence of transforming the properties of the tilted disk into the observed coordinates and intensities.

We formulate our model in § II. This formulation is then used to generate synthetic H I line profiles for comparison with the observations, which are described in § III. The predictions inherent in the model are tested against the observational material in §§ IV–VII. In § IV, we consider moment maps of integrated H I intensity as these appear projected onto the plane of the sky. In § V, we show intensity contours in an l, v map constructed along the major axis of the observed fundamental gas distribution, emphasizing the kinematic symmetry revealed by these data and the consequent availability of an inner-Galaxy rotation curve. Section VI is concerned with the observed and predicted behavior in 10 representative l, v maps each at a different latitude; similarly, four b, v maps are discussed in § VII. In § VIII we point out two curious features that apparently represent opposed streams of material flowing outward along the polar axis of the tilted disk. In § IX we summarize the observational features subsumed by the model, discuss some suggested revisions to earlier views of various inner-Galaxy phenomena, and speculate briefly on the effects of a massive, precessing central disk on the Galaxy at large. In Paper II, we judge the model in the context of molecular observations in the central region of the Galaxy.

It is worth remarking that the observational situation is more definite in a number of respects for our own galactic nucleus than for other nuclei. Thus the direction and distance of our nucleus are known rather accurately, so that crucial z-distances for inner-Galaxy material, which follow directly from latitude angles, are firm to $\pm 15\%$. Potential ambiguities of the sort problematic in other galaxies because of errors in the adopted inclination do not exist in the present case: the Galaxy at large is viewed edge-on, and the inclination of the inner-Galaxy disk can be measured, as discussed below, with no sign ambiguity. Similarly, potential ambiguities involved in separating expanding from contracting material are resolved by the possibility of absorption against the nuclear continuum sources and by several other criteria discussed below.

II. THE TILTED-DISK MODEL OF THE FUNDAMENTAL GAS DISTRIBUTION

The observations reveal in a variety of ways that the fundamental distribution of the gas in the inner Galaxy describes a tilted disk, within which the gas kinematics involve both rotation and expansion. It might seem logical to point out the relevant observational characteristics before formulating the model. However, because these characteristics take such a variety of forms, we can put them in the context of the model more easily if we describe it first. In practice, the choice of the parameters defining the model required some iterative comparisons between observed and simulated profiles.

The orientation of the disk is specified by two angles. The position angle, α, measures the angle in the plane of the sky between the rotation axis of the Galaxy and that of the disk. The inclination, i, measures the angle between the plane of the sky and the equatorial plane of the disk. If the apparent major axis of the disk coincides with $b = 0°$, then $\alpha = 0°$; α increases if the latitude of the positive-longitude part of the disk decreases. If the disk is viewed edge-on, then $i = 90°$; i decreases if the latitude of the near part of the disk decreases. The angle between the axis of the disk and that of the Galaxy is $\cos^{-1}(\sin i \cos \alpha)$. By analogy with the usual galactic coordinates, we specify perpendicular distance from the disk axis by ϖ_d, expansion velocities in the ϖ_d direction by Π_d, perpendicular distance from the central plane of the disk by z_d, and rotation velocities orthogonal to both the ϖ_d and z_d directions by Θ_d. Π_d is positive for motions in the direction of increasing ϖ_d; Θ_d is positive for motions in the direction of galactic rotation. The disk has azimuthal symmetry, so that Π_d and Θ_d depend only on the radius ϖ_d. The gas density, n_d, is constant at a given z_d, and its dependence on z_d is of Gaussian form specified by a scale height h_d. The radial extent of the disk is ϖ_d'.

Location and motion in the Galaxy itself also enter our calculations, and are specified by ϖ, $\Theta(\varpi)$, ϕ, and z. The galactic azimuth, ϕ, is measured in the direction of rotation from the Sun-center line. The galactic-layer scale height is h, and the total radial extent of the Galaxy is ϖ'. At the Sun's location, we use $\varpi_0 = 10$ kpc and $\Theta_0 = 250 \text{ km s}^{-1}$.

Figure 1 shows the projection of the fundamental disk in galactic coordinates. The drawing is done to scale, using the values $\alpha = 22°$, $i = 78°$, $\varpi_d' = 1.5$ kpc, and $h_d = 0.10$ kpc. We might save the reader some confusion if we point out immediately that although the disk is symmetric in both azimuth and z_d, and is concentric with the Galaxy, it will never show symmetry in the observational (l, b), (l, v), or (b, v) coordinates. This lack of symmetry appears in several ways in Figure 1. For example, the region of the disk closer to the Sun appears at more extreme b than the more distant part. It also appears thicker in b.

For a point at a distance r from the Sun on a line of sight in the direction (l, b), conversion to the disk coordinates gives

$$z_d = \varpi_0 \cos i + r[\sin i (\sin b \cos \alpha + \cos b \sin l \sin \alpha) - \cos i \cos b \cos l] \tag{1}$$

and

$$\varpi_d = (r^2 + \varpi_0^2 - 2\varpi_0 r \cos l \cos b - z_d^2)^{1/2} . \tag{2}$$

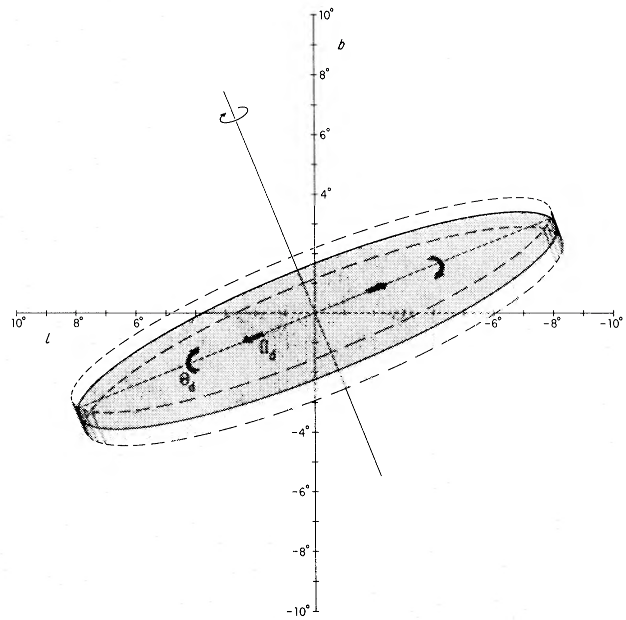

FIG. 1.—Appearance of the model tilted gas distribution as projected onto the plane of the sky in angular coordinates. The solid-line approximate ellipse represents the equatorial plane, where $z_d = 0$ pc, of a disk of radius $\varpi_d' = 1.5$ kpc tilted through the angles defined in the text: $\alpha = 22°$ and $i = 78°$. The axis of the disk and the axis of the Galaxy form a 25° angle. The dashed lines correspond to the disks at heights $z_d = \pm 100$ pc. The vectors indicate schematically the rotation function $\Theta_d(\varpi_d)$ and the expansion function $\Pi_d(\varpi_d)$.

We consider the point to lie within the disk if

$$\varpi_d < \varpi_d' \tag{3}$$

and if

$$|z_d| < 3h_d \, .$$

The gas density at the point is

$$n_d = n_0 \exp\left[-\tfrac{1}{2}(z_d/h_d)^2\right] , \tag{4}$$

where n_0 is the density in the plane $z_d = 0$ kpc. The velocity at the point measured with respect to the local standard of rest is

$$\begin{aligned} v_d = {} & \Pi_d(\varpi_d)[\varpi_d^2 - \varpi_0(\varpi_0 - r\cos b\cos l - z_d \cos i)](\varpi_d r)^{-1} \\ & - \Theta_d(\varpi_d)\varpi_0 \sin i\,(\sin b \sin\alpha - \cos b \sin l \cos\alpha)/\varpi_d - \Theta_0 \sin l \cos b \, . \end{aligned} \tag{5}$$

The kinematic functions Π_d and Θ_d used below are

$$\Pi_d(\varpi_d) = 170[1 - \exp(-\varpi_d/0.07)] \text{ km s}^{-1} , \tag{6}$$

and

$$\begin{aligned} \Theta_d(\varpi_d) & = 180[1 - \exp(-\varpi_d/0.20)] \text{ km s}^{-1} && \text{if } \varpi_d \le 0.85 \text{ kpc} \\ & = 180\{1 - \exp[-(1.7 - \varpi_d)/0.20]\} \text{ km s}^{-1} && \text{if } \varpi_d > 0.85 \text{ kpc} \, . \end{aligned} \tag{7}$$

The magnitude and form of Π_d follow most directly from observations taken near $l = 0°$, so the detailed specification of this function is left to Paper II which deals with much higher-angular-resolution observations of carbon monoxide. As outlined below in § V, Θ_d can be directly derived from observations taken along the major axis of the disk, i.e., from the locus $b = -l \tan\alpha$.

In some calculations we included the contribution of gas lying in the usual galactic layer. Thus for the line-of-sight location (l, b, r), if the double condition (3) is not fulfilled, we find instead

$$z = r \sin b \tag{8}$$

and

$$\varpi = (r^2 + \varpi_0^2 - 2\varpi_0 r \cos l \cos b)^{1/2}, \tag{9}$$

and then test if

$$\varpi < \varpi' \tag{10}$$

and if

$$|z| < 3h .$$

When condition (10) is fulfilled, the gas density is

$$n = n_0 \exp\left[-\frac{1}{2}\left(\frac{z}{h}\right)^2\right]; \tag{11}$$

otherwise, $n = 0\ \mathrm{cm}^{-3}$. The radial velocity at the point is, familiarly,

$$v = \varpi_0[\Theta(\varpi)/\varpi - \Theta_0/\varpi_0] \sin l \cos b . \tag{12}$$

Kinematics, rather than the gas density or temperature distributions, dominate the appearance of low-latitude spectra of ubiquitous galactic tracers like H I and CO (see Burton 1971, 1972). It is difficult to understand all of the predictions inherent in a model except by generating synthetic spectra. This is certainly true in the present case, because the behavior of the crucial kinematic variables v_d and dv_d/dr at various positions along various lines of sight is not readily apparent. The synthetic spectra generated here include the consequences of radiative transfer inherent in the model velocity field and gas and density distributions.

We have specified the free parameters of the model by requiring agreement between synthetic and observed spectral characteristics, while attempting to keep the model as simple as possible. The only parameters we adjust are those defining the geometry of the tilted distribution and the motions within it. Thus the geometrical free parameters α, i, ϖ_d', and h_d are all constants, and the kinematic free function $\Pi_d(\varpi_d)$ and $\Theta_d(\varpi_d)$ are relatively uncomplicated functions of ϖ_d only. The physical parameters of the gas were not varied at all, but were taken over unchanged from investigations of the Galaxy at large. The gas density and temperature parameters are from Baker and Burton (1975): $n_0 = 0.33\ \mathrm{cm}^{-3}$ and $T_s = 120$ K. The velocity dispersion of the gas is taken from an extrapolation to the galactic center of equation (12) of Burton (1971), i.e., $\sigma = 9\ \mathrm{km\ s}^{-1}$. The synthetic-profile calculation followed the procedure outlined by Burton (1971). Because of the smooth variation of all parameters, a synthesized line-beam suffices. All parameters relevant to the modeling process are summarized in Table 1.

III. OBSERVATIONAL MATERIAL

The observational material with which we confront the model consists of 21 cm spectra of H I emission from the region $349° \leq l \leq 13°$, $-10° \leq b \leq 10°$. Burton, Gallagher, and McGrath (1977) observed this region at 1° angular intervals to a 3 σ rms sensitivity of 0.2 K. We have incorporated their data with additional spectra measured on the same grid, in order to improve the sensitivity, and have doubled the total number of spectra from the region by observing at the half-degree grid points in latitude. The new observations were made during 1977 January and February, using the NRAO 140 foot (43 m) telescope. The telescope was equipped with a cooled parametric amplifier of 50 K system temperature and a 384-channel autocorrelation spectrometer of 5 MHz total bandpass. After dropping the extreme 20 channels (unusable because of the non-square response of the bandpass), the instrumental baseline was accounted for by removing a polynomial of order 3 or less, determined

TABLE 1

PARAMETERS OF THE FUNDAMENTAL GAS DISTRIBUTION IN THE INNER GALAXY AND IN THE GALAXY AT LARGE

For the inner-Galaxy disk where $\varpi_d < \varpi_d'$ and $\lvert z_d\rvert < 3h_d$:	
Position angle	$\alpha = 22°$
Inclination	$i = 78°$
Radial extent	$\varpi_d' = 1.5$ kpc
Scale height	$h_d = 0.10$ kpc
Expansion	$\Pi_d(\varpi_d) = 170[1 - \exp(-\varpi_d/0.07)]\ \mathrm{km\ s}^{-1}$
Rotation	$\Theta_d(\varpi_d) = 180[1 - \exp(-\varpi_0/0.20)]\ \mathrm{km\ s}^{-1}$ if $\varpi_d \leq 0.85$ kpc
	$\Theta_d(\varpi_d) = 180\{1 - \exp[-(1.7 - \varpi_d)/0.20]\}\ \mathrm{km\ s}^{-1}$ if $\varpi_d > 0.85$ kpc
For the Galaxy at large where $\varpi < \varpi'$ and $\lvert z\rvert < 3\ h$:	
Radial extent	$\varpi' = 15.0$ kpc
Scale height	$h = 0.12$ kpc if $\varpi < 9.5$ kpc; otherwise $h = 0.12 + 0.023(\varpi - 9.5)$ kpc
Mean height of layer	$z_0 = 0.0$ kpc if $\varpi < 9.5$ kpc; otherwise $z_0 = 0.12(\varpi - 9.5)\cos(\phi - 85°)$ kpc
Rotation	$\Theta(\varpi)$ given by Burton and Gordon (1978)
For the H I everywhere in the Galaxy:	
$n_0 = 0.33\ \mathrm{cm}^{-3}$, $T_s = 120$ K, and $\sigma = 9\ \mathrm{km\ s}^{-1}$	

from least squares fitting to portions of the bandpass judged by separate inspection of each profile to contain negligible emission. Because the new material was taken using the same equipment and observational procedure as used by Burton *et al.*, a homogeneous data set resulted when we combined the material.

The observations give coverage of the velocity range $-500 < v < 500$ km s^{-1}, with velocities expressed throughout this paper with respect to the local standard of rest defined by the standard solar motion of 20 km s^{-1} toward α, $\delta = 18^{\text{h}}$, $+30°$ (epoch 1900.0). Digital smoothing degraded the velocity resolution to 11 km s^{-1}, but enhanced the sensitivity of the data to an rms level of 0.03 K. To maintain this level uniformly, longer integration times were necessary in directions where continuum radiation sources raised the total system temperature. Thus at $l, b = 0\overset{\circ}{.}0, 0\overset{\circ}{.}0$, an integration time of 5240 s was required to achieve the same rms level as typically achieved elsewhere after 320 s of integration. We express measured intensities in terms of antenna temperature; Lindblad (1974) discusses the relationship between antenna temperature measured on the 140 foot telescope and brightness temperature.

A compilation of the observational parameters of presently current sets of 21 cm data of the general region of the galactic center is given by Burton *et al.* The combined material used here is superior to earlier work in terms of the very broad velocity coverage, in the sensitivity, and in the breadth of its positional coverage. Because the density of the coverage is not high, the $\Delta b = 0\overset{\circ}{.}5$, $\Delta l = 1\overset{\circ}{.}0$ grid interval sets the angular resolution.

IV. APPEARANCE OF THE FUNDAMENTAL GAS DISTRIBUTION IN MOMENT MAPS

The most obvious measure of the emission centroid of the inner-Galaxy gas is provided by the integrated-intensity first moment. Because of its anomalous kinematics, this gas may be separated to a large degree from other line-of-sight material by suitable choice of the range of integration. The moment maps are also convenient at the beginning of the modeling process because they are relatively insensitive to the otherwise dominant kinematic functions Π_d and Θ_d, but do reflect the input values of ϖ_d', α, and i rather directly.

Figure 2 shows contours of observed antenna temperatures integrated over the range $-300 < v < -99$ km s^{-1}. For the case of pure galactic rotation, no emission is predicted at $l > 0°$ in this velocity range. That forbidden-velocity emission is observed indicates $\Pi_d \neq 0$, and its absorption in front of the Sagittarius continuum source indicates $\Pi_d > 0$ km s^{-1}. At $l < 0°$, the integrated emission is contributed by both forbidden- and allowed-velocity material, but essentially all of the forbidden-velocity gas lies in a coherent distribution, tilted with respect to the plane $b = 0°$ and crossing the plane $l = 0°$ at negative latitude. Figure 3 shows an analogous situation for the positive-velocity gas. Plotted in that figure are intensities integrated over the range $99 < v < 300$ km s^{-1}, which is forbidden at $l < 0°$. Essentially all of this forbidden-velocity gas also lies in a coherent tilted distribution, crossing the plane $l = 0°$ at positive latitudes.

For comparison with Figures 2 and 3, we show in Figure 4 the moments calculated over the same velocity ranges using the model gas distribution described in § II; emission from the Galaxy at large is also included in Figures 4*c* and 4*d*. Even restricting the velocity range to $|v| \geq 100$ km s^{-1} clearly does not isolate the inner-Galaxy contribution except within $|l| \lesssim 2°$. Contamination by transgalactic emission causes the higher-level contours to be symmetric with respect to $b = 0°$, but the situation represented by the lower-level contours is less confused.

The modeled moment distributions show the same general trends as are observed, including the zero-longitude crossings at $b \neq 0°$, as well as the tilted nature and extent of the moment distributions. They also show that a direct reading of the tilted-disk parameters from either observed moment map (as from other observational displays) can be misleading. Thus, in Figure 4, a direct measurement of the tilt of the modeled moment distribution does not yield $\alpha = 22°$, just as the apparent longitude extent of the distribution is less that expected solely from calculating $\sin^{-1}(\varpi_d'/10 \text{ kpc})$.

V. KINEMATIC SYMMETRIES ON THE LINE $b = -l \tan \alpha$: THE ROTATION FUNCTION $\Theta_d(\varpi_d)$

Spectral data from the central region of our Galaxy are mostly displayed either in l, v maps taken parallel to the plane $b = 0°$ or in b, v maps taken parallel to $l = 0°$. For gas distributed as in Figure 1, such cuts are not the most physically revealing. The line crossing the disk in that figure is the projection, after tilting, of the disk diameter running perpendicular to the line of sight through the galactic center in the case $\alpha = 0°$, $i = 90°$. (Note that this projected diameter is neither the exact major axis of an ellipse—cuts through the circular disk at constant z_d not projecting to ellipses—nor a straight line.) This locus is approximately $b = -l \tan \alpha$, and in terms of the model a position-velocity map constructed along it should reveal the maximum extent of the tilted distribution. Such a map also should show a high degree of kinematic symmetry about its origin (because the projections of the functions Θ_d and Π_d onto the line of sight are very nearly antisymmetric about $l = b = 0°$, $v = 0$ km s^{-1}), and so should yield straightforward information about the rotation and expansion functions in the inner Galaxy. Finally, this map has the advantage over the usual one at $b = 0°$ that there is less contamination from foreground and background material in the Galaxy at large, owing to the typically large $|z|$.

For these reasons, we show in Figure 5 an observational l, v map on the line $b = -l \tan \alpha$, as provided by interpolation within the observed grid. To avoid distortion of the contours caused by absorption at the position of the galactic center, we have replaced the spectrum at that point by the average of those at $l, b = 0\overset{\circ}{.}0, +0\overset{\circ}{.}5$ and $0\overset{\circ}{.}0, -0\overset{\circ}{.}5$. As predicted, and in great contrast to the corresponding map taken only at $b = 0°$, the observations

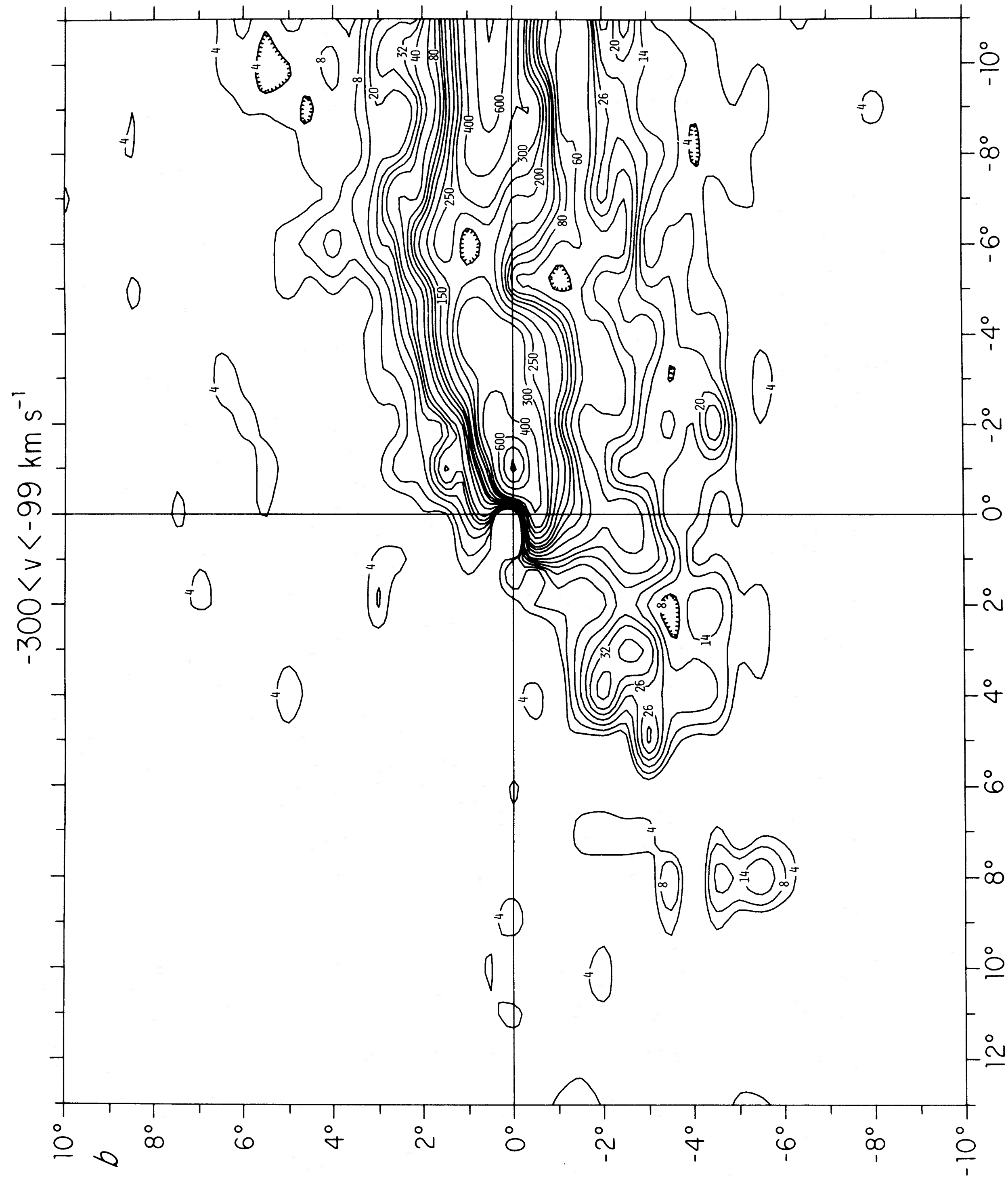
-300 < v < -99 km s^{-1}
b
l
10°
8°
6°
4°
2°
0°
-2°
-4°
-6°
-8°
-10°
12°

now show a high degree of kinematic symmetry about the origin of the map. That the envelope of the emission is not pinched toward $v = 0 \text{ km s}^{-1}$ at $l = 0°$ indicates radial motion; that the pattern is skew indicates rotation. Very close to the galactic center, the expansion function dominates the kinematics. The negative-velocity H I absorption (cf. Fig. 2) against the Sagittarius continuum sources then shows directly that the radial motion is expansion rather than contraction. The extent of the emission envelope in Figure 5 indicates that a maximum value of 170 km s^{-1} is appropriate for Π_d: in choosing such a value, we allow for the additional profile broadening due to the internal dispersion σ. The chosen maximum value represents a compromise between the negative- and positive-velocity extents of the envelope which, at $l = 0°$, are slightly displaced (~ 15 km s^{-1}) to positive velocities. The most direct explanation of this displacement, and one which is indicated even more strongly by the CO observations discussed in Paper II, is that the dynamical center of the disk is offset slightly to negative longitudes. As stated above, specification of the expansion function is left to Paper II, which deals mainly with observations of the innermost disk material. However, the specific choice of the expansion as given in equation (6) influences each display of the synthetic spectra presented in this work; there are consequently many opportunities to test it against the present observations.

An expansion function having been adopted, the behavior of the rotation motion can be found rather directly by requiring the terminal velocities present in synthetic profiles to match those actually observed. Because expansion is present, and because the disk is tilted, the largest values of v along the lines of sight used in the fitting arise not at the subcentral point but elsewhere, depending on the detailed behavior of Θ_d. Thus, some iteration was required, but no adjustments were made in order to suit the observations away from the line $b = -l \tan \alpha$.

The adopted Π_d and Θ_d functions are shown in Figure 6, along with the rotation curves of Sanders and Lowinger (1972) and Burton and Gordon (1978). Obviously the presence of large expansion velocities forces our rotation curve to be much smaller in magnitude than those previously employed. We mention below several tests of the validity of equation (6) and equation (7); in particular, see Figure 9 and our discussion of it in the following section.

The synthetic maps generated along the line $b = -l \tan \alpha$ are shown in Figures 7*a* and 7*b*, where, in the latter, we have also included the contribution of the Galaxy at large. We can generally separate the inner-Galaxy material from the foreground and background gas on the basis of kinematic criteria which are valid because of the known and well-behaved kinematics of the Galaxy at large: in Figure 7*b*, for instance, emission from the general galactic layer dominates only for $|v| \leq 60 \text{ km s}^{-1}$, because $b \neq 0°$ generally. Subtraction in one's mind's eye of contaminating emission can be done for all of the observational figures in this paper, focusing attention on the inner-Galaxy gas, and so facilitating comparison of the observational characteristics with those modeled, excluding transgalactic contributions.

In comparing Figures 5 and 7, heaviest weight should be given to the agreement of the outer envelopes of the distributions. This agreement indicates that the kinematics are successfully modeled. The intensities are less important, especially because the intensity levels at large $|v|$ in the observational figure, and the structure in them, are diminished through interpolation within the coarse observed grid. Thus we suspect that the modeled intensity ridges apparent in Figure 7 are smoothed out by the large variations perceived in the disk between 1° grid intervals.

VI. APPEARANCE OF THE FUNDAMENTAL DISTRIBUTION IN l, v MAPS

In this section we compare with the observations the appearance of the model gas distribution in 10 l, v maps constructed at constant galactic latitudes. Maps are shown at enough latitudes to demonstrate the changing behavior of the disk signature and to enable us to remark on a variety of features, previously studied separately, which are accounted for solely by the present description of the inner-Galaxy material.

The observed spectra are represented in Figure 8 by contours of antenna temperature drawn at the levels $T_A = 0.11, 0.23, 0.4, 0.9, 1.7, 3.0, 6.0, 10.0, 16.0, 25.0, 35.0, \ldots$ K. The lowest-level contour is 4 times the typical rms noise; inspection of it provides a good criterion for the interpretation of weak features. The latitude of each map is shown in the upper left corner together with an indication of its location with respect to the model distribution (the dashed lines in the schematic disks refer to the heights $z_d = \pm h_d$). Plotted as dashed lines and superposed on the observations are contours representing brightness temperatures in the synthetic spectra at the levels 0.1, 0.4, 1.8, 3.8, 7.0, 11.0, 16.0, 24.0, ... K, but for the sake of clarity these are not labeled. In any case, detailed comparison of the observed antenna temperatures with model values of the brightness temperature is usually not as relevant to our purposes as comparison of the more general locations and trends in the data and model distribution. The synthetic profiles exclude the Galaxy at large. In the observed data, the contribution of such material should be mentally subtracted within the band $|v| < 100 \text{ km s}^{-1}$.

FIG. 2.—Contours of observed antenna temperature integrated over the velocity range $-300 < v < -99 \text{ km s}^{-1}$, and projected onto the plane of the sky. Material in this velocity range is "forbidden," at $l > 0°$, in terms of circular differential galactic rotation. Absorption due to the Sgr A complex indicates that the bulk of the negative-velocity material in the direction $l, b = 0°, 0°$ has a net motion away from the center of the Galaxy.

1978ApJ...225..815B

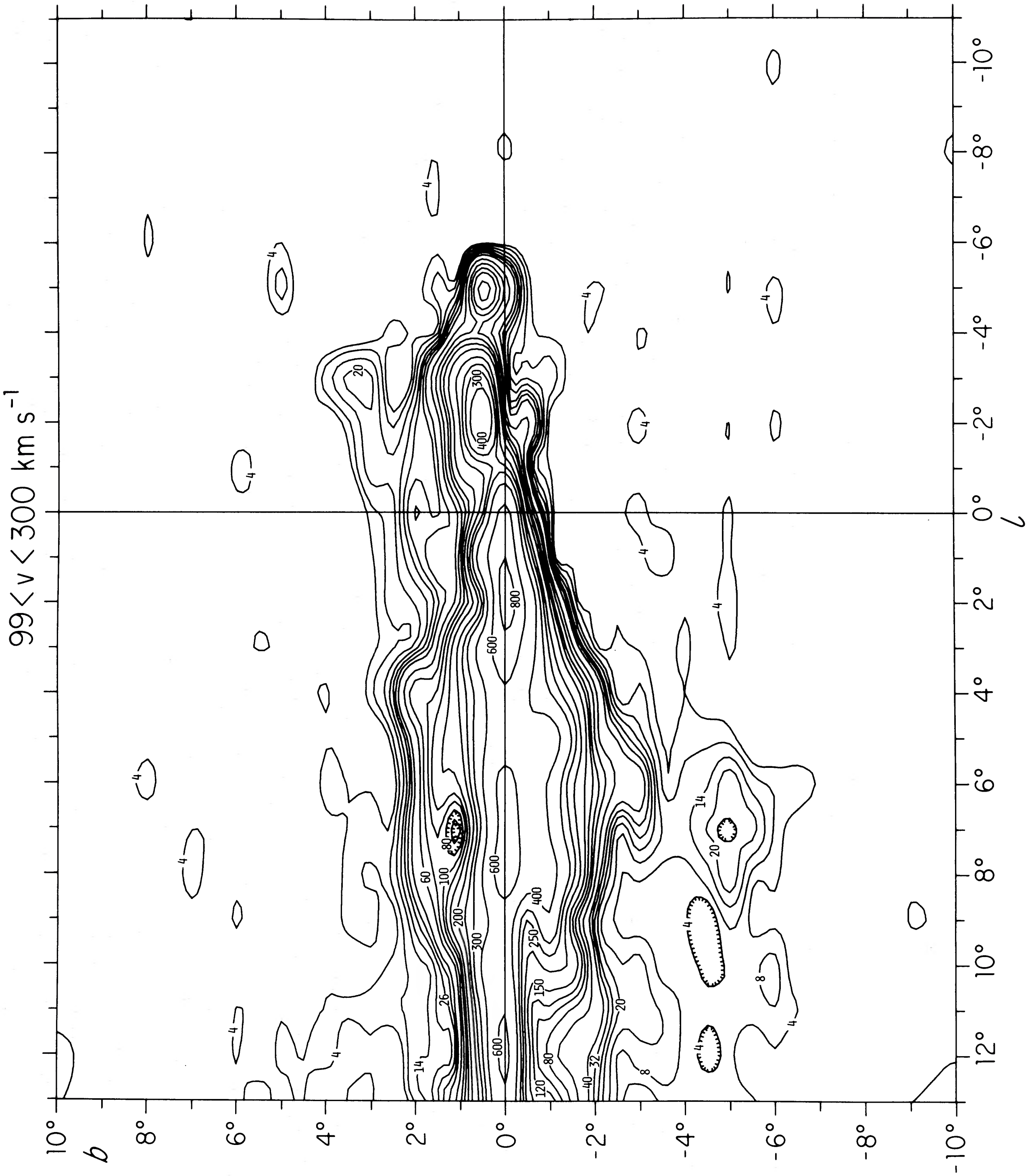

The l, v map at $b = +4°.5$, Figure 8*a*, intersects the inner-Galaxy material at such large values of z_a that the intensities are very weak: such an almost null case is useful in giving an impression of the expected foreground and background contributions. Viewed in the context of the following figures, however, it seems likely that the contour excursion near $l = -6°$, $v = -100$ km s^{-1} is a manifestation of the disk.

The map at $b = +3°.0$, shown in Figure 8*b*, is the first in this series which intersects regions in the disk having substantial densities. The signature of the model encompasses the observed perturbations. The positive-velocity extension has been the subject of several separate studies. Sanders and Wrixon (1972*b*) consider the material near $l = -3°$, $v = 100$ km s^{-1}, to be a jet of gas expelled from the galactic nucleus by pressure of cosmic rays from Sgr A, and comment on its apparent alignment with ridges of 1.5 GHz continuum emission reported by Kerr and Sinclair (1966). Cohen (1975; see also Cohen and Davies 1976) discussed the higher velocity gas near $l = -1°$ separately under the name feature J2, but does relate it to the Sanders and Wrixon feature—as indeed seems required by the present data. The combined feature plays an important role in Oort's (1977) interpretation, where it is considered to be a definite example of a feature with ejective origin.

In Figure 8*c*, representing $b = +2°.5$, the positive-velocity observations show features VII of van der Kruit (1970), feature J2 of Cohen (1975), and the Sanders and Wrixon (1972*b*) feature, all of which are adequately encompassed by the model. Particularly relevant in the present context is the observed negative-velocity disk extension. As far as we know, this feature has not been discussed separately, perhaps because it lies in an "allowed" quadrant or because it lies outside the range of most earlier surveys. It corresponds in our model to the outer reaches of the disk on its far side. Its slope in the l, v plane is a consequence of a decrease in rotation speed in the outer parts of the disk. The feature at $l = 4°$, $v = 120$ km s^{-1}, has not been discussed before and is not accounted for by our synthesis.

Figures 8*d*, 8*e*, and 8*f* show emission from the l, v planes at $b = +0°.5$, $0°.0$, and $-0°.5$, respectively, where lines of sight traverse long paths through the Galaxy. Figure 9 shows the synthetic-profile emission at $b = -0°.5$—qualitatively similar to those at $b = 0°.0$ and $b = 0°.5$—for the combined contribution of gas in the inner-Galaxy tilted disk as well as in the general galactic layer. At these latitudes the 3 kpc arm appears in the observations as a very regular band crossing $v = -100$ km s^{-1} at $l = -8°$; its contribution should be ignored here because our discussion does not deal with it.

The appearance of individual features is obscured within 1° of the galactic equator. However, Figures 8*d*, 8*e*, and 8*f* do reveal several manifestations of the disk. One observed general characteristic is the shift of the major pattern crossing zero velocity, from $l < 0°$ at $b = +0°.5$, through $l = 0°$ at $b = 0°$, to $l > 0°$ at $b = -0°.5$. This is not compatible with symmetry with respect to the galactic equator, but is accounted for by the geometry of our model. The synthetic disk signature at $|b| \leq 0°.5$ comprises several regions of enhanced emission which extend over some 6°–8° in longitude, all of which, in our model, arise solely from the behavior of v_a given by equation (5). The observations show similarly elongated features, but interpretation of them in terms of arc-like density concentrations is central to most analyses (see the review by Oort 1977). For example, Cohen and Davies (1976) extrapolate a number of the observed features over arcs in the l, v plane in order to find their tangential directions and galactocentric distances.

The most crucial of the extended features appearing in the low-latitude observations is the "rotating nuclear disk" which heretofore has provided the conventionally accepted gravitational potential for the region between 50 and 800 pc from the galactic center. In the observations, it is the ridge of emission crossing zero velocity near $l = 0°$. Rougoor and Oort (1960), and subsequently many others, have interpreted this crossing as a signature of rotation. The suddenness with which the "rotating nuclear disk" appears to cross zero velocity is, of course, enhanced by absorption against the central continuum sources in Sgr A, a phenomenon which forces closure of iso-intensity contours in l, v maps and diminishes the perceived intensity of gas at $v < 0$ km s^{-1}, $0° \leq l \leq 1°$ (cf. Cohen 1977 and Sanders, Wrixon, and Mebold 1977). We have tried to minimize the influence of absorption in Figure 8*e* by substituting an average profile for that taken at $l = b = 0°$, but absorption undoubtedly contributes to the low intensities observed at higher (positive) longitudes. The presence of positive velocity absorption against Sgr A at 40 km s^{-1} (e.g., Sandqvist 1974) is easily produced in our model if the continuum sources lie even slightly beyond the midplane of the model distribution or if they lie even 1′–2′ to more positive longitudes than does the disk center.

A puzzling aspect of the original interpretation of the "rotating nuclear disk" has been the general lack of a positive-longitude, positive-velocity continuation. This lack of kinematic symmetry, which in the inclined-disk context we do not expect in the plane $b = 0°$, has previously required an asymmetric gas distribution, with the separation of a half ($l < 0°$) which is rotating and at higher density from one of lower density in which rotation does not play a dominant role. In turn, the lack of symmetry of the central density distribution is difficult to explain, given the strong gravitational field that has been assumed to exist. Also, the existence of the classical rotating disk precisely up to $l = 0°$, but not beyond, forces the Sun into a favored location in the Galaxy. These

FIG. 3.—Contours of observed antenna temperatures integrated over the velocity range $+99 < v < +300$ km s^{-1}, and projected onto the plane of the sky. Material in this velocity range is "forbidden," at $l < 0°$, in the terms of circular differential galactic rotation.

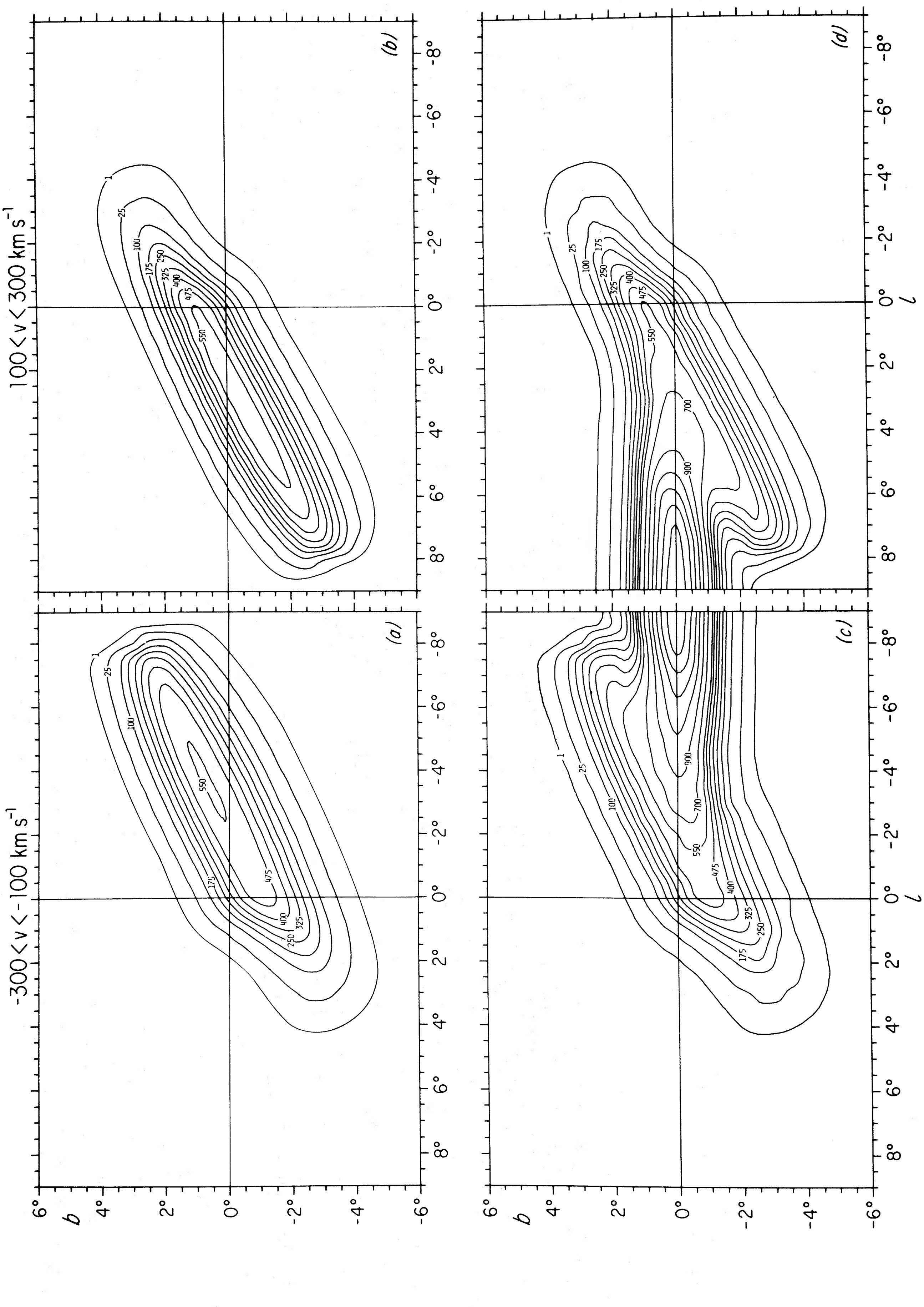
100 < v < 300 km s^-1
-300 < v < -100 km s^-1
(a)
(b)
(c)
(d)
b
l

difficulties are adequately and coherently eliminated in the present synthesis which, though it is dominated by expansion motions in the very innermost regions, nonetheless produces a pattern in l, v space like that which has previously been interpreted as arising from rotation alone. As evidenced by the gray contours in Figures 8*d*, 8*e*, and 8*f*, and in Figure 9, one need not introduce locally enhanced volume densities into the model to account for the ridge of emission under discussion here, for it arises naturally as the result of the velocity fields which are present. If enhanced intensities were interpreted as locally enhanced volume densities—erroneously in this case and in others pointed out below—the observations might then be taken to infer the existence of a central feature such as a bar (cf. Kerr 1967 and Cohen and Davies 1976), arc (Sanders and Wrixon 1973), or spiral arm (Sanders, Wrixon, and Mebold 1977). Our model, in which density varies only with scale height, produces an intensity contrast between the "rotating nuclear disk" and the nearby emission which is at least as great as that actually observed (compare our Fig. 9—representing $b = -0\overset{\circ}{.}5$, and, qualitatively, $b = 0\overset{\circ}{.}0$ and $+0\overset{\circ}{.}5$—with Fig. 1 of Sanders *et al.*). We conclude that there is no compelling evidence for any separate feature occurring close to the galactic center.

Figure 8*g* shows another example of an extended and apparently armlike feature in the l, v plane, extending at $b = -1\overset{\circ}{.}5$ from $v = 240$ km s^{-1}, $l = 3°$ to $v = 140$ km s^{-1}, $l = 8°$. It is the "connecting arm" of Rougoor (1964), feature III of van der Kruit (1970) and feature IIIa of Cohen (1975). Different interpretations are given by Rougoor (1964), Kerr (1967), van der Kruit (1970), and Cohen and Davies (1976). The most problematic characteristic of this feature is its contrary tilt in the l, v plane: to account for this, Kerr and also Cohen and Davies invoked a central bar distribution, and Rougoor invoked a steeply inclined spiral feature. Our model adequately accounts for the "connecting arm" feature; the unusual tilt of the pattern is a consequence of the decrease of Θ_d at $\varpi_d > 1.0$ kpc.

The modeled contours at positive velocities in Figure 8*g* enclose—in addition to the connecting arm pattern—a broad region in l, v space with little variation in intensity. This region encompasses the supposedly separate feature J4 of Cohen (1975). Cohen's description of the feature is entirely consistent with the manner in which our synthesis subsumes it: according to him, feature J4 extends from $l = 2°$ to $l = 5°$; it has an exceptionally large velocity half-width; its l, v pattern points away from the galactic nucleus; and, finally, it is difficult to isolate from the surrounding emission.

A feature found by Sanders, Wrixon, and Penzias (1972), labeled E, also plays a central role in the interpretation of galactic nucleus phenomena. It is characterized observationally (cf. Figs. 8*g*, 8*h*, and 8*i*) by a negative latitude, an $l = 0°$ crossing at $v = -170$ km s^{-1}, a velocity half-width of 40–50 km s^{-1}, and a small change of velocity with longitude. In Oort's review, E is considered one of the most definite examples (together with J2; see Fig. 8*b*) of a compact, jetlike, gas cloud ejected from the nucleus. In our synthesis, which accounts for these observational parameters in detail, the characteristics of feature E are straightforward attributes of the velocity and geometrical projections of the fundamental inner-Galaxy gas kinematics and distribution.

At $b = -2\overset{\circ}{.}5$ (Fig. 8*h*), the positive-velocity pattern near $l = 6°$ is Cohen's feature J4. Cohen (1975) and Cohen and Davies (1976) note that J4 lies on a ridge in l, b space (see Fig. 3) whose alignment suggests collimated ejection from the galactic nucleus, but our model also predicts a general alignment (see Fig. 4*b* and the insert in Fig. 8*h*). The negative-velocity portion of the observed l, v plane at $b = -2\overset{\circ}{.}5$ shows the combined emission from features X, XII, and E, as well as from an unnamed feature discussed by Sanders, Wrixon, and Penzias (1972). The modeled negative-velocity pattern is confined in velocity over much of its extent and shows a strong gradient dl/dv. These factors have contributed to the interpretation of the disk signature as separate features when viewed previously in the more common b, v maps.

The ability of the model to represent the observations is quite important at latitudes representing z-distances of more than several hundred parsecs. Figure 8*i* shows the observed and predicted emission in the l, v plane at $b = -3\overset{\circ}{.}0$: such an angle corresponds to a linear distance greater than 500 pc at the galactic center. The positive-velocity emission represents Cohen's apparently blended features J4 and J5; the negative-velocity behavior does not differ much from that at $b = -2\overset{\circ}{.}5$. It is interesting, however, to compare the $b = -3\overset{\circ}{.}0$ situation with that at the corresponding positive latitude in Figure 8*b*. The two (l, v)-plane patterns observed are approximately symmetric, but the negative-latitude pattern is more pronounced, as predicted.

Comparison of Figure 8*j*, representing $b = -4\overset{\circ}{.}5$, with Figure 8*a*, representing $b = +4\overset{\circ}{.}5$, also shows a relative enhancement of the negative-latitude emission. There is just a hint of the disk pattern at $b = +4\overset{\circ}{.}5$, while at $-4\overset{\circ}{.}5$ it remains pronounced. This behavior is predicted by the model because the nearer portions of the disk subtend a noticeably larger solid angle than those which are more distant. It is also one of several indications that the sign of the inclination-angle parameter is correct. The negative-velocity portion of the disk signature encompasses

FIG. 4.—Arrangement on the plane of the sky of intensities integrated over the indicated velocity ranges in synthetic spectra representing H I in the modeled inner-Galaxy distribution. (*a*) and (*c*) The moment map calculated over the range $-300 < v < -100$ km s^{-1}. (*b*) and (*d*) The moment map calculated over the range $+100 < v < +300$ km s^{-1}. Parts (*a*) and (*b*) of this figure exclude the contribution from the Galaxy at large; parts (*c*) and (*d*) include it. The synthetic moment maps can be compared with the observational ones in Figs. 2 and 3. The moment maps are quite sensitive to the parameters α, i, $\varpi_{d'}$; they are less sensitive to the detailed form of Θ_d or Π_d.

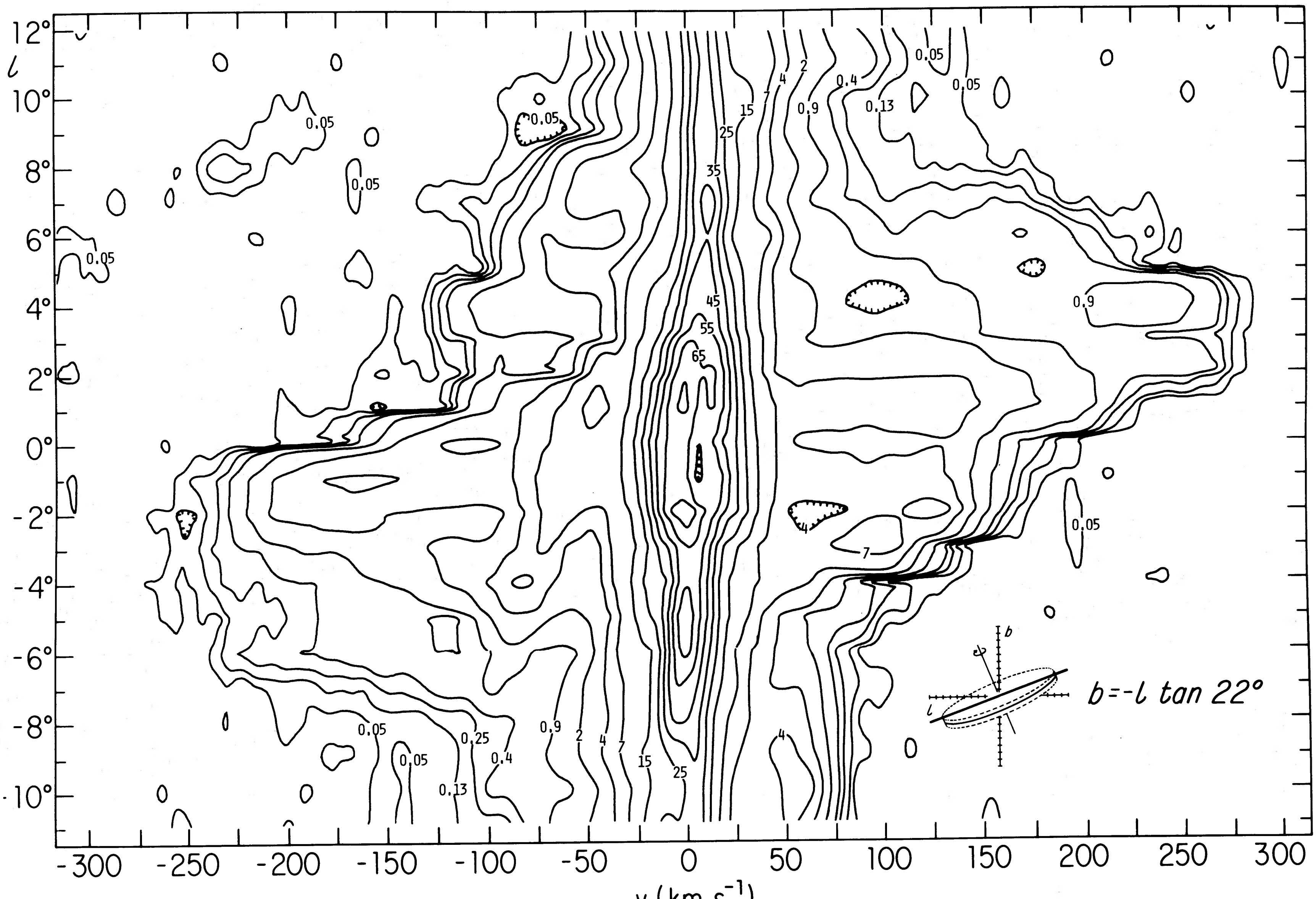

FIG. 5.—Longitude, velocity arrangement of emission observed from the direction $b = -l \tan 22°$. This cut through the inner Galaxy reveals the approximate extent of the tilted fundamental distribution of gas, and shows the high degree of kinematic symmetry present.

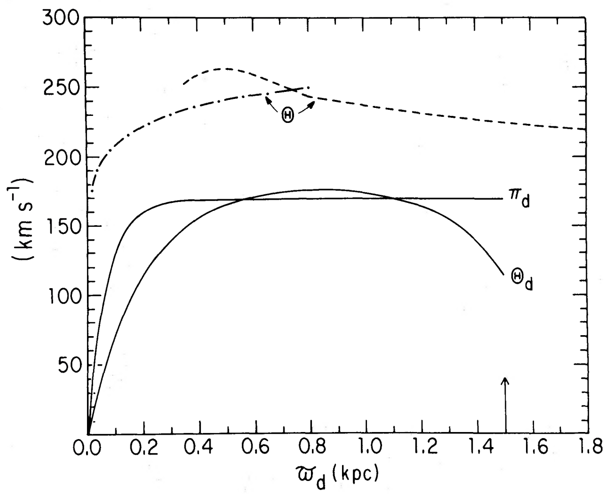

FIG. 6.—Rotation and expansion in the tilted disk. *Solid lines*, the rotation and expansion functions, Θ_d and Π_d, used in this paper. *Dot-dash line*, the rotation curve derived by Sanders and Lowinger (1972). *Dashed line*, the rotation curve of Burton and Gordon (1978). Note the slower rotation which results in this work when the presence of a general expansion component is included. The derivation of Θ_d is discussed in § IV.

most of the observational characteristics which motivated Sanders and Wrixon (1972*a*) to postulate a complete expanding and rotating ring of gas 2.4 kpc from the galactic center.

Two features observed near $b = -4\overset{\circ}{.}5$ are not accounted for by the model. These are Sanders and Wrixon's (1972*a*) feature (cf. Cohen's J1) at $l = -3°$, $v = -140$ km s^{-1}, which may be an extension of the higher-longitude emission pattern, and Shane's clearly separated feature (see Oort 1968; Hulsbosch 1968; Saraber and Shane 1974) near $l = 8°$, $v = -220$ km s^{-1}. We note that both features lie in the fundamental plane described by the disk model, but that an explanation in terms of the disk requires that we accept the existence of anomalies near its boundaries. Regarding Shane's feature, we note that a change in the sign of the projected model velocity is expected near the longitude termination of the disk (which is also near the $b = -4\overset{\circ}{.}5$ intersection). The velocities predicted by the model are, however, not sufficiently large in this region to provide a straightforward association with the observed feature.

One general characteristic shared by the features which are not subsumed by the model is a rather small velocity dispersion, ~ 10 km s^{-1}, and in this sense they differ from those features which find a natural explanation in the present work. Shane's feature in particular resembles many examples of high-velocity clouds, which are unrelated to the inner-Galaxy phenomena under discussion here. Identification of Shane's feature with a high-velocity cloud requires, however, that its alignment with the disk's fundamental plane be fortuitous.

VII. APPEARANCE OF THE FUNDAMENTAL DISTRIBUTION IN b, v MAPS

Each of the four sections of Figure 10 shows the observed and modeled emission from a b, v cut at a constant l. These maps are on the whole less useful in the present context than those presented in l, v coordinates because the b-extent of the disk is less than its l-extent, and because each constant-l cut traverses the contaminating layer of the Galaxy at large. They are useful to the extent that they show the deviation of the emission centroid of the inner-Galaxy disk from the equatorial plane $b = 0°$. Figures 10*a*, 10*b*, 10*c*, and 10*d* show, respectively, emission from the b, v planes at $l = 4\overset{\circ}{.}0$, $2\overset{\circ}{.}0$, $-2\overset{\circ}{.}0$, and $-4\overset{\circ}{.}0$. The modeled contours indicate that the observed shifts of the emission cen roid at velocities corresponding to inner-Galaxy material are adequately accounted for. The figure legends indicate which of the observational features, previously considered isolated, are encompassed by the model; of particular interest in view of the earlier interpretations (see Oort's review) is the material previously described as feature E, evident in Figure 10*b* at negative velocities. The emission pattern projecting to negative latitudes in Figure 10*c* has been interpreted as representing expulsion from the nucleus at a high angle with respect to the galactic plane. Feature J2 occurs in the same figure at positive velocities, and, in view of its apparent large angle with respect to the nucleus, it also has been considered expelled gas.

VIII. THE SPECULATIVE POLAR-AXIS STREAMS

Figure 11 shows contours of antenna temperature integrated over the velocity ranges $-300 < v < -41$ km s^{-1} at $l > 0°$, and over the range $41 < v < 300$ km s^{-1} at $l < 0°$. The observations reveal two elongated features which do not lie in the fundamental plane of the model gas distribution. The negative-velocity moment map shows a weak but evidently coherent stream entering the observed space near $l = 13°$, $b = 10°$, and running to

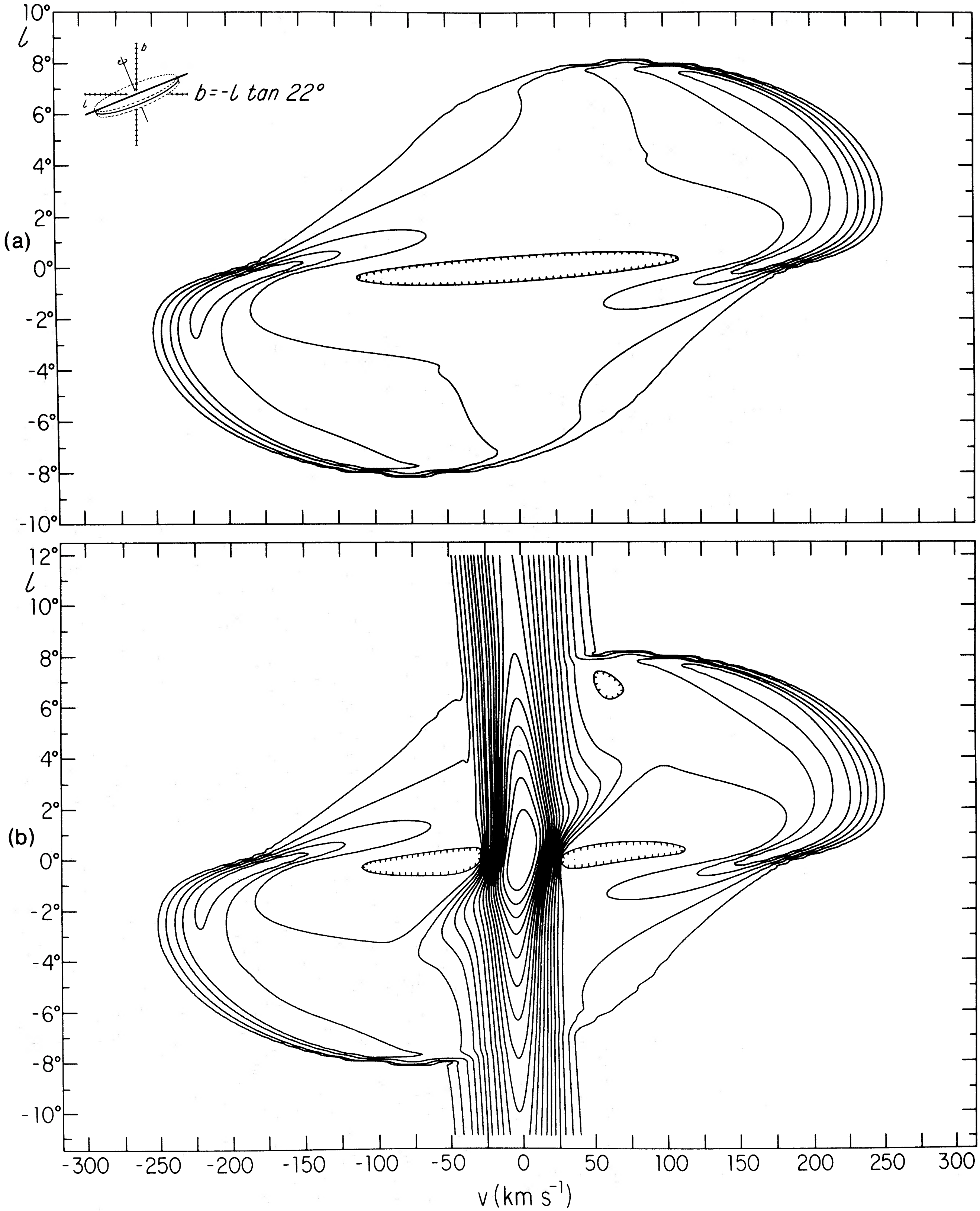

FIG. 7.—Longitude, velocity arrangement of emission in synthetic profiles as calculated at directions for which $b = -l \tan 22°$. (*a*) The situation for gas lying only in the inner-Galaxy distribution. (*b*) The situation for gas in the Galaxy at large, as well as in the inclined disk.

TABLE 2

SPECIFIC OBSERVATIONAL FEATURES SUBSUMED BY THE TILTED-DISK MODEL OF THE INNER-GALAXY H I DISTRIBUTION

Observational Feature	Earlier Interpretations	Principal References	Representative Position: l (°)	Representative Position: b (°)	Representative Position: v (km s^{-1})	Comparison Figures in This Paper
"Nuclear disk," vdK IV	Rapidly rotating disk; gives inner-Galaxy mass distribution	1, 2, 5, 11, 12, 14	$0 \rightarrow -4$	$0.5 \rightarrow -0.5$	< -50	8*d*, *e*, *f*; 9
"Nuclear disk," SW d and e	Rotating ring; steeply inclined spiral arm	10, 13	$0 \rightarrow -4$	0.0	< -100	8*e*, *f*; 9
"Connecting arm," vdK III, C IIIa	Extensive high-pitch spiral arm; central bar	1, 2, 4, 5, 6, 11, 12, 14	>2	$0 \rightarrow -1$	>100	8*f*; 9
vdK XIV, C XIVa	Southern counterpart of connecting arm; III and XIV make up opposed branches of central bar or spiral	4, 5, 6, 11, 12	<2	0.5	< -150	8*d*
vdK XVI; SWM g	Gas inside nuclear disk; H I counterpart of "molecular ring" (see Paper II)	5, 11, 13	$1 \rightarrow 0.5$	0.0	170	8*d*, *e*
SW f	Expanding arm within rotating nuclear disk	10, 13	0.5	$0.0 \rightarrow -0.5$	-100	8*e*, *f*; 9
C J4	High-velocity jet from nucleus	11, 12	$5 \rightarrow 2$	$-1 \rightarrow -3$	120	8*g*, *h*; 10*a*
C J5	High-velocity jet from nucleus (cf. J4)	11, 12	$8 \rightarrow 2$	-3	110	8*i* (cf. J4 in 8*g*, *h*)
SWP E	Prototype of jetlike consequence of explosive event; high angle to plane $b = 0°$	8, 9, 14	$2 \rightarrow -1$	$0 \rightarrow -4$	-160	8*g*, *h*, *i*; 10*b*
SW, C J2	Isolated cloud expelled from nucleus at high angle; associated with 20 cm jets	3, 4, 8, 11, 12, 14	$-1 \rightarrow -3$	3	100	8*b*, *c*; 10*c*
vdK XII	Prototype of arm-line consequence of explosive event	5, 6, 7, 11, 12, 14	$9 \rightarrow -3$	$-1 \rightarrow -3$	-100	8*g*, *h*, *i*; 10*a*
vdK VII	Evidence of nuclear activity	5, 11, 14	$0 \rightarrow -4$	$-1 \rightarrow -3$	85	8*c*; 10*c*
vdK X	Expanding feature whose high *z*-distance indicates ejection from nucleus	5, 11, 12, 14	$5 \rightarrow -2$	$-2 \rightarrow -3$	-120	8*h*; 10*a*

REFERENCES.—(1) Rougoor and Oort 1960. (2) Rougoor 1964. (3) Kerr and Sinclair 1966. (4) Kerr 1967. (5) van der Kruit 1970. (6) van der Kruit 1971. (7) Sanders and Wrixon 1972*a*. (8) Sanders and Wrixon 1972*b*. (9) Sanders, Wrixon, and Penzias 1972. (10) Sanders and Wrixon 1973. (11) Cohen 1975. (12) Cohen and Davies 1976. (13) Sanders, Wrixon, and Mebold 1977. (14) Oort 1977.

$l = 0°$, $b = 3°$, where it blends with other emission. The mean projected velocity of this stream is -45 ± 10 km s^{-1}. Knots of emission within it have previously been pointed out by van der Kruit (1970, cf. XIII), Cohen (1975, cf. J3), and by d'Odorico *et al.* (1969). The corresponding positive-velocity moment map[1] shows, at negative latitudes, a comparable stream of hydrogen extending from the blended region near $l = 0°$, $b = -6°$ to the boundary of the observed space at $l = -6°$, $b = -10°$. This feature was first noticed by Mirabel and Turner (1975) at $l < -1°$ and followed to $l = -10°$, $b = -22°$. The mean projected velocity over its entire observed extent is $+45 \pm 10$ km s^{-1}.

Although we have no direct information on the distance or nature of these two streams, the several similarities between them are quite striking. Both show the same speed, constant over most of their extent, and have similar velocity dispersions, peak intensities (and so column densities), and spatial distributions. They are oriented approximately parallel to the polar axis of the inner-Galaxy disk, suggesting an association with the galactic nucleus. For these reasons, we find it not unreasonable to speculate that the two streams represent opposed steady flow outward from the galactic nucleus along the rotation axis of the disk, with a flow velocity of magnitude 45 km s^{-1}/cos i = 216 km s^{-1}. Because the sign of the inclination is not likely to be in error, the flow is directed outward, and the polar-axis streams are not indicative of a circulation source for outflowing disk material. In the portion of the northern polar-axis stream encompassed by the observed grid, we find $M_{\rm H\,I} = 3 \times 10^5\ M_\odot$ assuming the gas to be optically thin and confined to a $13° \times 1.°5$ band at 10 kpc distance. Because the stream extends beyond our grid, its total H I mass is undoubtedly larger. The H I mass of the southern polar-axis stream, as estimated out to $b = -22°$ by Mirabel and Turner (1975), is $2.5 \times 10^6\ M_\odot$.

[1] Material described by Cugnon (1968; see also Mirabel, Pöppel, and Vieira 1975) is present in Fig. 11, but we see no relationship between it and the inner-Galaxy phenomena described here. Although Cugnon's feature lies near the fundamental plane of our disk, it has a mean velocity, ~ 50 km s^{-1}, much smaller than suggested by an extension of our model, and shows little of the expected disk signature. Cugnon's feature also cannot be explained by warping of the outer galactic layer if the description of this warp given by Baker and Burton (1975) is correct. That description (see Table 1) invokes a small excursion from $b = 0°$ at the relevant longitudes (cf. Fig. 4*d*).

FIG. 8*a*.—Emission in the l, v plane at $b = +4.°5$. This cut intersects the inner-Galaxy tilted disk far above its mean plane and consequently shows only a weak disk signature.

FIG. 8*b*.—Emission in the l, v plane at $b = +3.°0$. The observed positive-velocity manifestation of the disk at $l = -3°$ was discussed as a separate entity by Sanders and Wrixon (1972*b*); the disk signature at higher positive velocities near $l = -1°$ is Cohen's (1975) separate feature J2.

FIG. 8*c*.—Emission in the l, v plane at $b = +2.°5$. The positive-velocity emission near $-1° < l < 0°$ at $v = 100$ km s^{-1} encompasses van der Kruit's (1970) feature VII and Cohen's (1975) feature J2, as well as a feature discussed by Sanders and Wrixon (1972*b*). The negative-velocity manifestation of the disk, near $l = 6°$, has not been discussed separately.

FIG. 8*d*.—Emission in the l, v plane at $b = +0.°5$. The appearance of individual features is obscured within 1° of the galactic equator by emission from the Galaxy at large. The model successfully accounts for the observed pattern shift to negative longitudes. Our discussion does not deal with the 3 kpc arm, which crosses $v = -100$ km s^{-1} at $l = -8°$ in the maps at $b = 0°$ and $\pm 0.°5$.

FIG. 8*e*.—Emission in the l, v plane at $b = 0.°0$. The negative-velocity, positive-longitude signature of the inner-Galaxy disk is damaged in the observations near $l = 0°$, $b = 0°$ by absorption against the strong continuum source in the galactic nucleus. In this figure the profile at $l = 0°$ is an average of those at $l = 0°$, $b = \pm 0.°5$. The feature at $l = -5°$, $v \approx 100$ km s^{-1} is not accounted for by our synthesis (H I: see Burton 1970; CO: see Bania's 1977 "clump 1").

FIG. 8*f*.—Emission in the l, v plane at $b = -0.°5$. As is the case with the cuts at $b = 0.°0$ and $+0.°5$, isolated features are obscured in this cut by the contribution of emission from the Galaxy at large (see Fig. 9). The extended feature at $l > 1°$, $100 < v < 250$ km s^{-1} is Rougoor's (1964) "connecting arm." The model successfully accounts for the overall trends in the observed distribution. The "rotating nuclear disk" feature near $l = 0°$ is accounted for but has, of course, a very different interpretation in the terms of the model.

FIG. 8*g*.—Emission in the l, v plane at $b = -1.°5$. The model contours encompass: Cohen's (1975) feature J4, in the vicinity of $l = 4°$, $v \approx 120$ km s^{-1}; van der Kruit's (1970) feature XII at $2° \leq l \leq 5°$, $v < 0$ km s^{-1}; the "connecting arm" of Rougoor (1964; cf. III*a* of Cohen 1975) at $l > 3°$, $100 \leq v \leq 250$ km s^{-1}; the minor feature V of van der Kruit and Cohen at $l = 0°$, $v = -110$ km s^{-1}; and feature E of Sanders *et al.* (1972) at $l < 0°$, $v \approx -180$ km s^{-1}.

FIG. 8*h*.—Emission in the l, v plane at $b = -2.°5$. The concentration of emission near $l = 6°$, $v = 160$ km s^{-1}, is accounted for by the model; it is Cohen's (1975) apparently isolated feature J4. The region at negative velocities contains, within the boundaries predicted by our synthesis, feature XII of van der Kruit (1970) at $3° < l < 6°$, $v \approx -50$ km s^{-1}; feature X of van der Kruit at $3° < l < 5°$, $v \approx -120$ km s^{-1}; feature E of Sanders *et al.* (1972) at $-2° < l < 2°$, $v \approx -160$ km s^{-1}; and a feature discussed separately by Sanders *et al.* (1972) at $1° < l < 3°$, $v \approx -90$ km s^{-1}. The observational distinction between these various features is not very clear, a point also consistent with our synthesis.

FIG. 8*i*.—Emission in the l, v plane at $b = -3.°0$. The emission concentration between $l = 5°$ and 8° at positive velocities in Cohen's (1975) feature J5; we see no way to distinguish it from his J4. Within the negative-velocity boundaries predicted by our model are the same features mentioned in the legend to Fig. 8*h*.

FIG. 8*j*.—Emission from the l, v plane at $b = -4.°5$. The disk signature at $b = 4.°5$ is predicted to be more pronounced than the one at the symmetric latitude $b = +4.°5$ (Fig. 8*a*) because the negative-latitude, positive-longitude portion of the disk is nearer the Sun. Note that at $|b| = 4.°5$, $|z| = 785$ pc at the distance of the galactic center. Cohen's (1975) feature J5 at $l \approx 7°$, $v \approx 100$ km s^{-1}, and van der Kruit's (1970) feature *X* at $2 < l < 5°$, $v \approx -100$ km s^{-1}, are inherent in the model. The negative-velocity disk signature lies on the locus of Sanders and Wrixon's (1972*a*) suggested ring of gas at $l = 2.4$ kpc. Shane's feature at $l = 8°$, $v = -220$ km s^{-1} and the Sanders and Wrixon (1972*a*) feature (J1 of Cohen 1975) at $l = -3°$, $v = -140$ km s^{-1} are not accounted for by the model, although both lie in the fundamental plane of the tilted disk. Shane's feature is discussed separately under the rubric "feature XI" by van der Kruit (1970), Cohen (1975), and Cohen and Davies (1976).

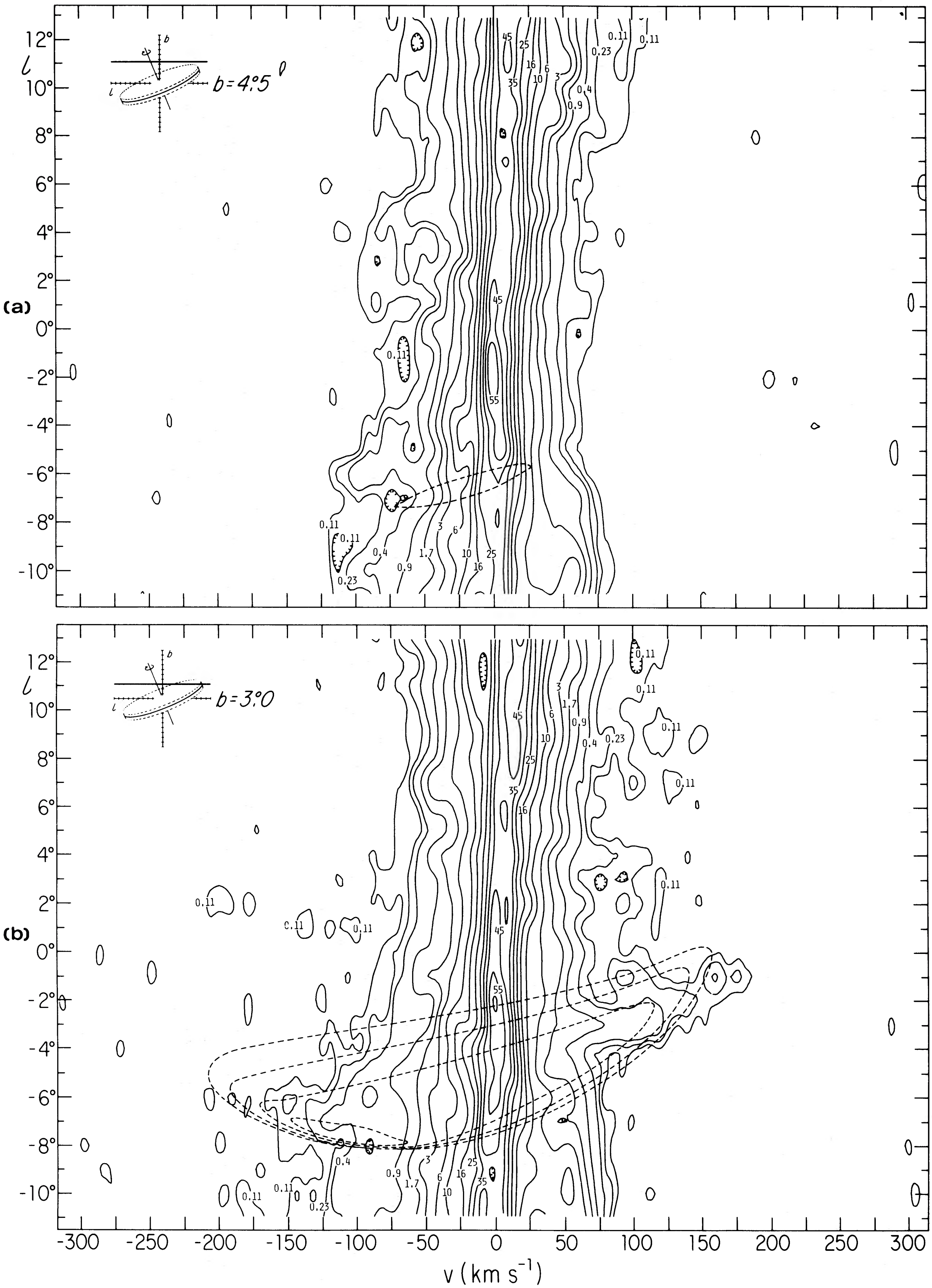
(a)
b=4°5
(b)
b=3°0
l
v (km s^{-1})

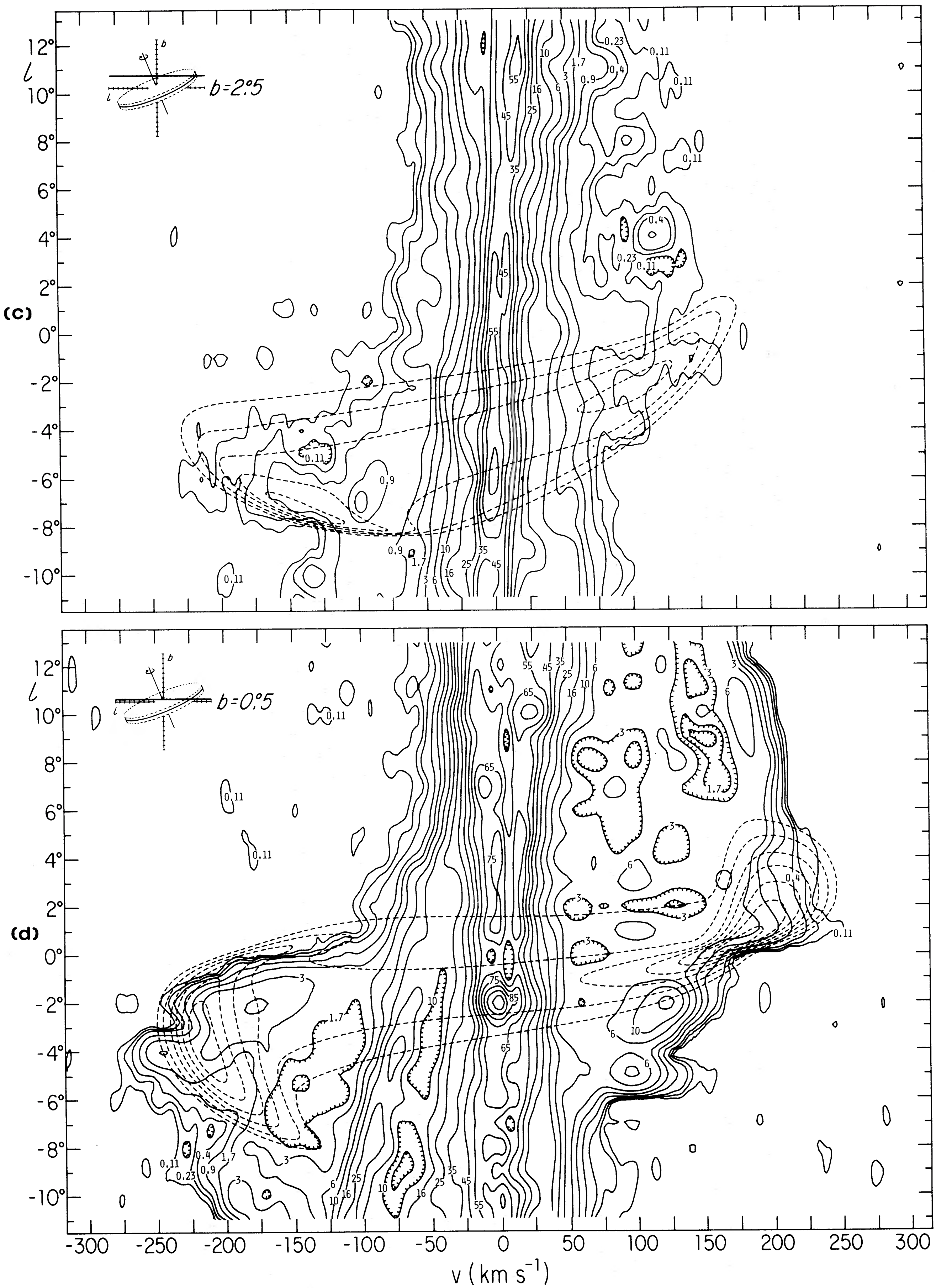
(c)
b=2°5
(d)
b=0°5
l
12°
10°
8°
6°
4°
2°
0°
-2°
-4°
-6°
-8°
-10°
-300 -250 -200 -150 -100 -50 0 50 100 150 200 250 300
v (km s^{-1})

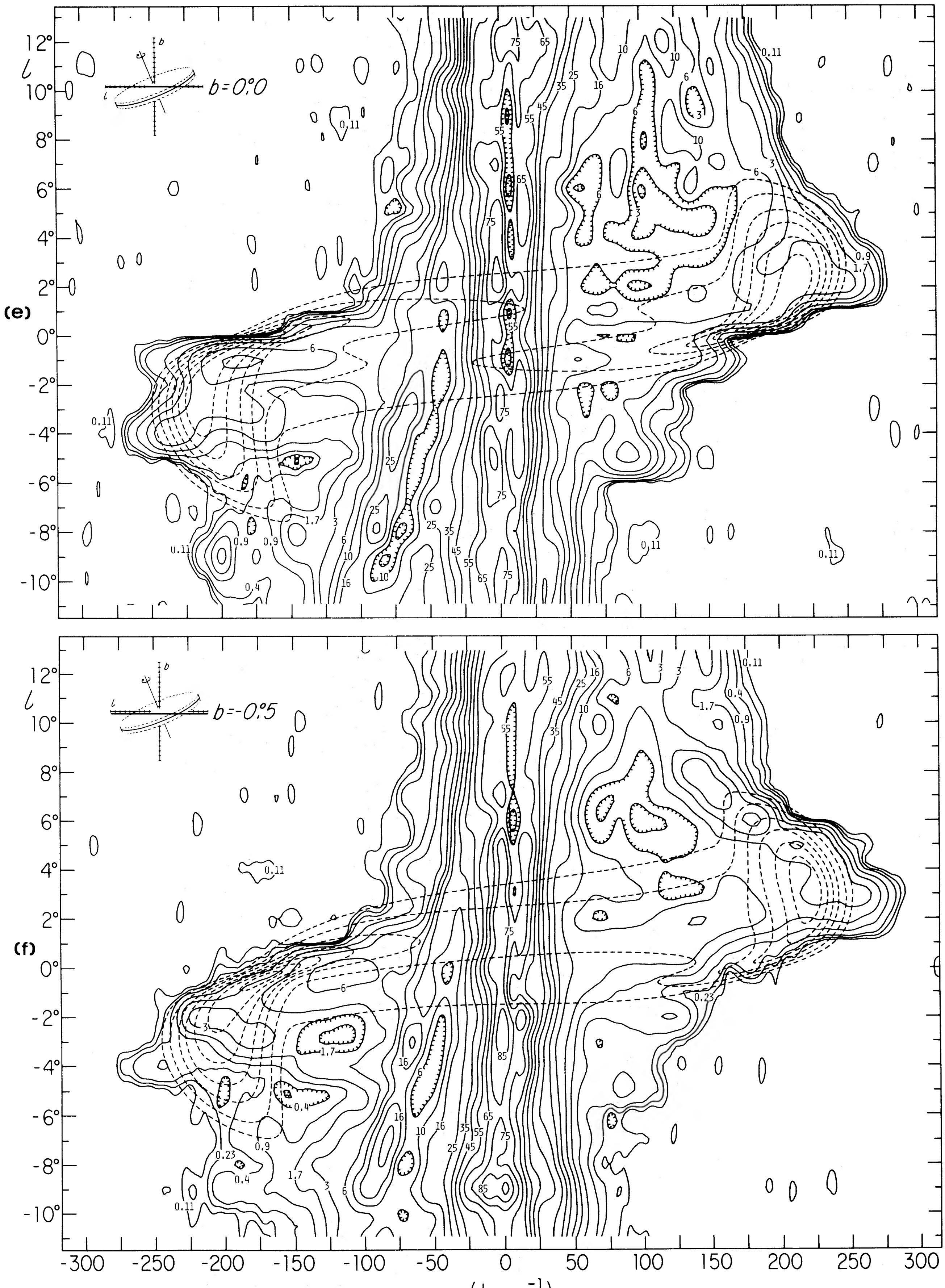
(e)
b=0°.0
(f)
b=-0°.5
12°
10°
8°
6°
4°
2°
0°
-2°
-4°
-6°
-8°
-10°
-300
-250
-200
-150
-100
-50
0
50
100
150
200
250
300
v (km s⁻¹)

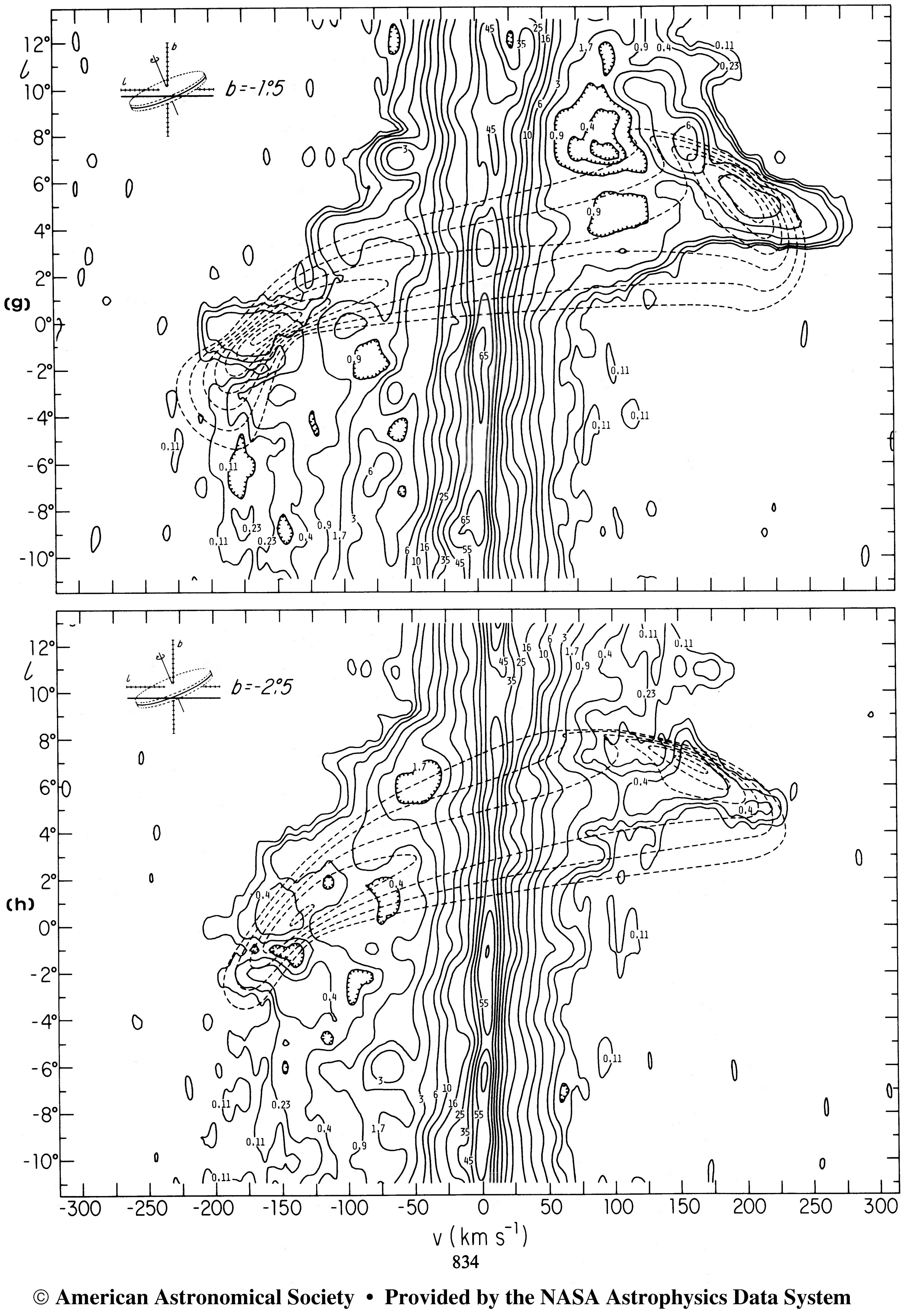
b=-1°5
(g)
b=-2°5
(h)
v (km s^{-1})

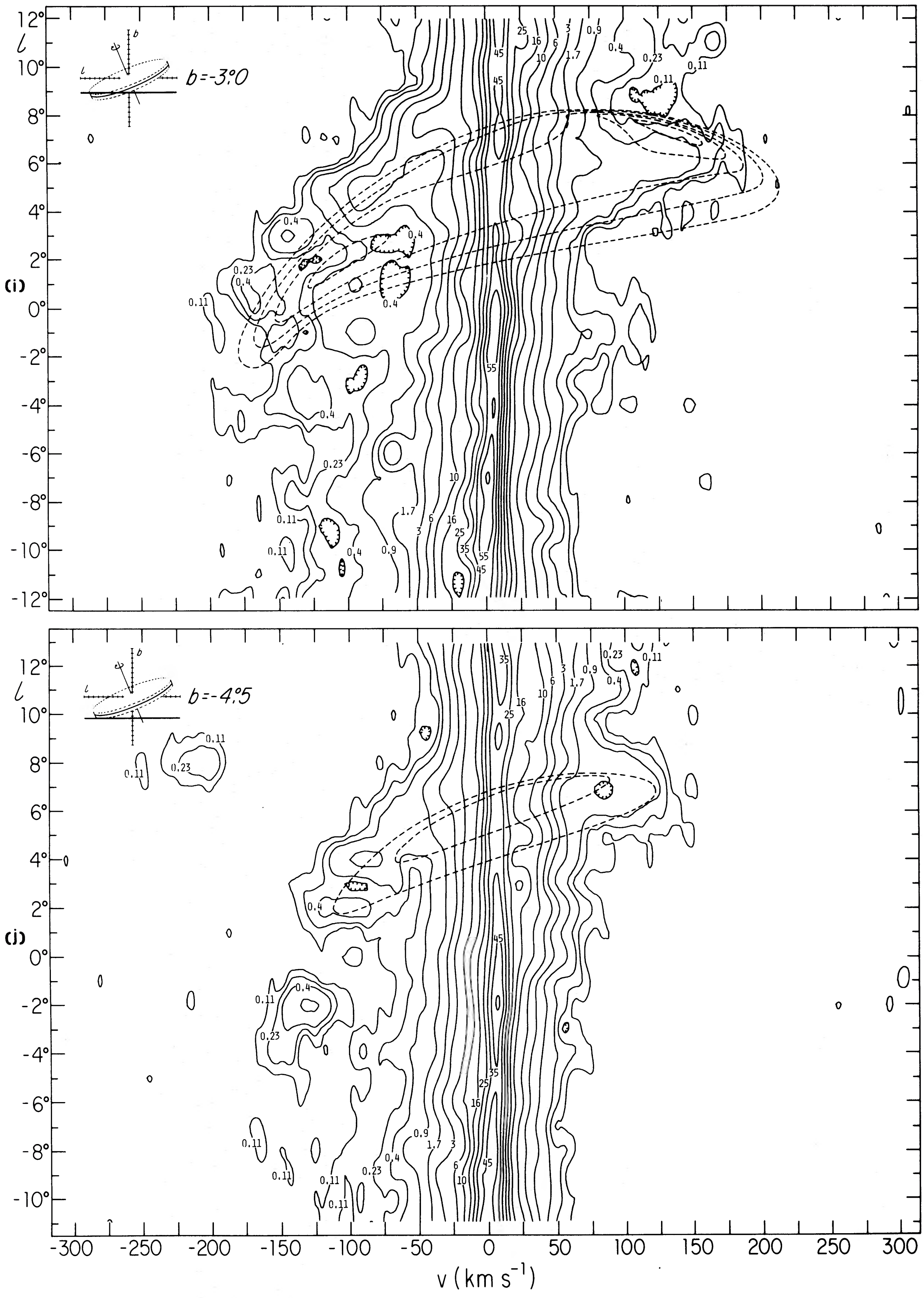

b=-3°0
(i)
b=-4°5
(j)
l
v (km s^-1)

1978ApJ...225..815B

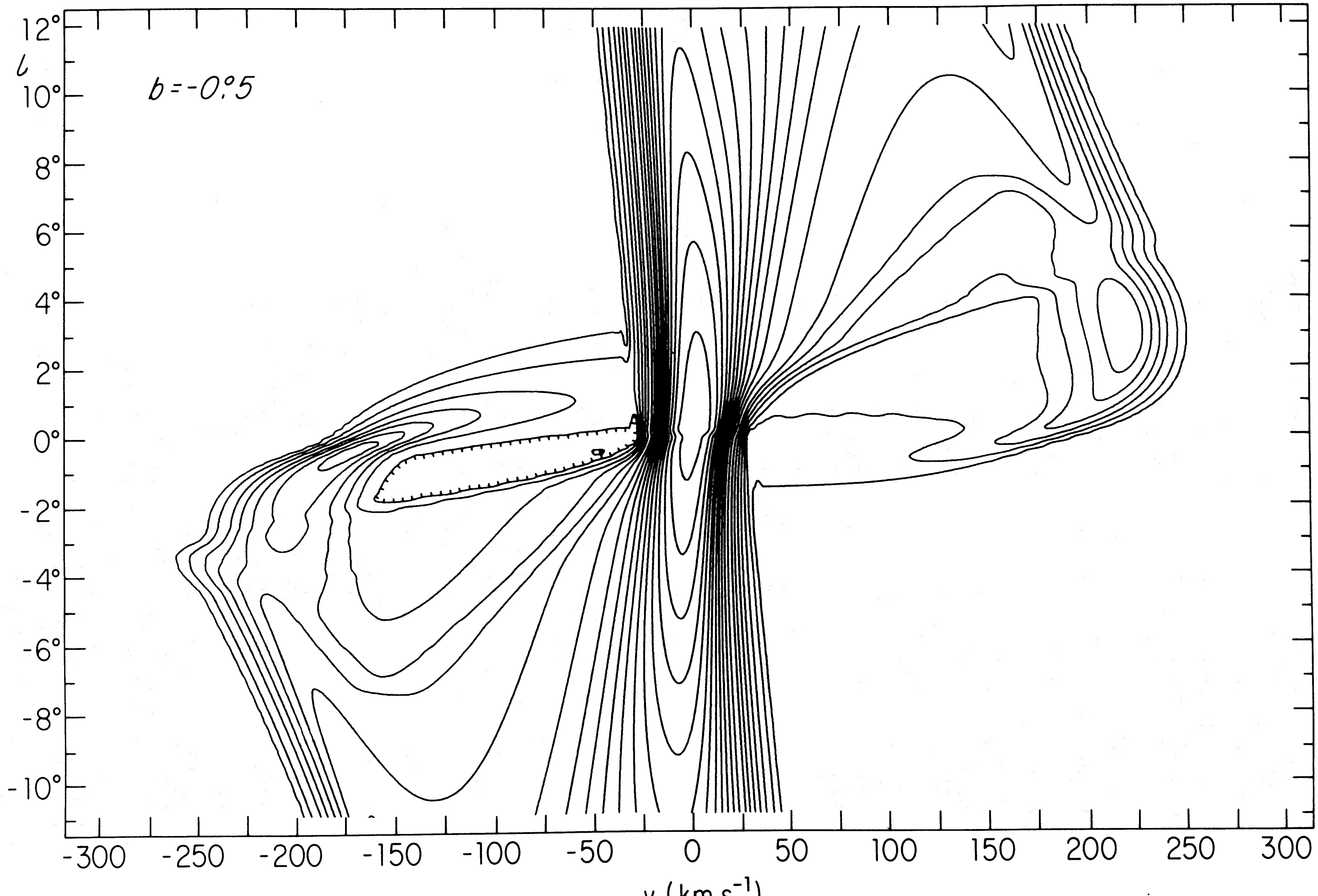

FIG. 9.—Synthetic-profile emission in the l, v plane at $b = -0°.5$, representing the combined contributions of gas in the inner-Galaxy disk and the model Galaxy at large. Comparison of this figure with Fig. 8f will help the reader to isolate the contribution of the disk in the low-latitude observations. This figure suggests that the tilted disk signature could easily be misinterpreted as a rapidly rotating, discrete, armlike feature. It also shows, as discussed in the text, that the combination of Θ_d and Π_d is compatible with the observational considerations which resulted in the detailed specification of the rotation curve Θ.

1978ApJ...225..815B

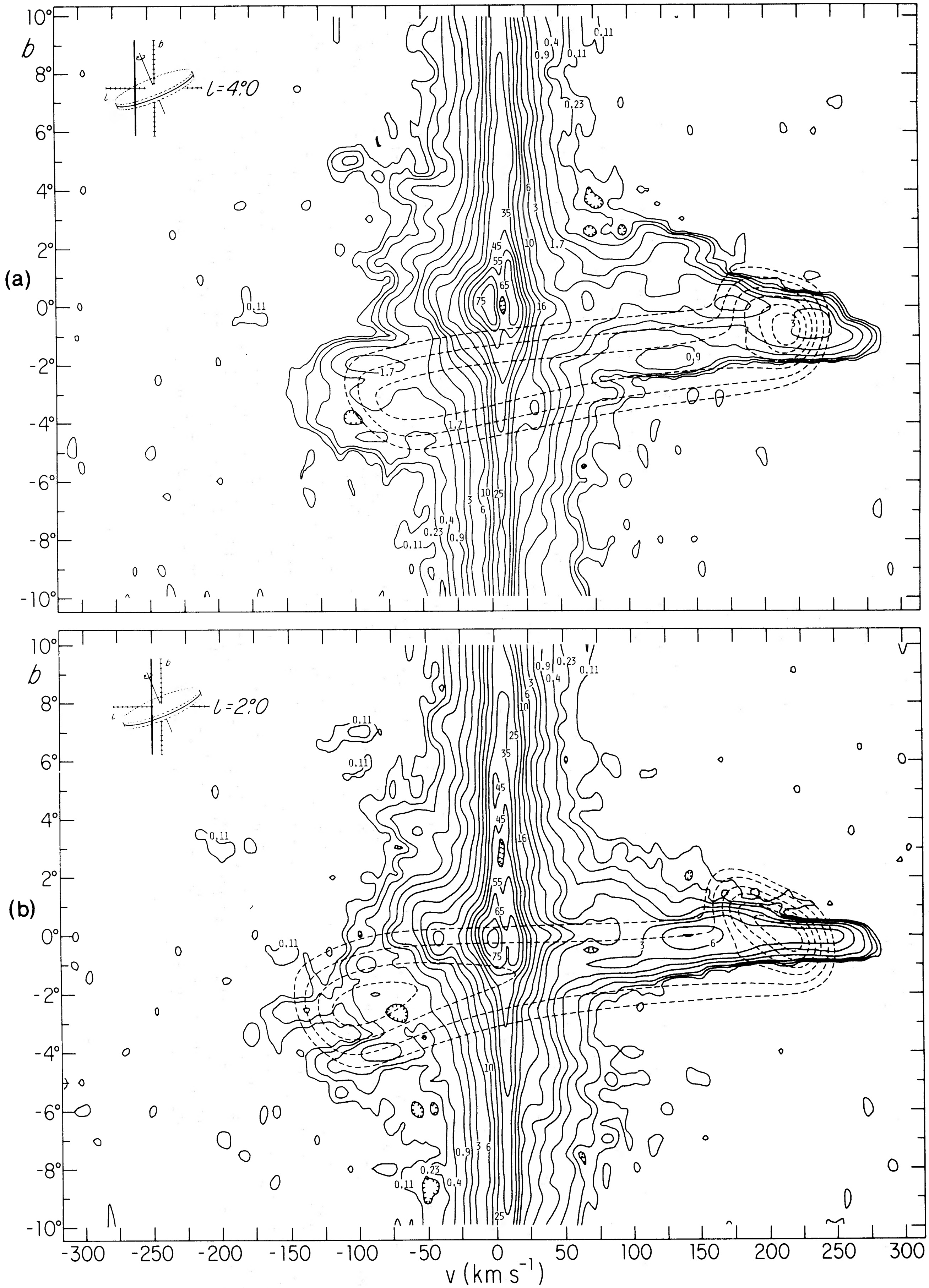

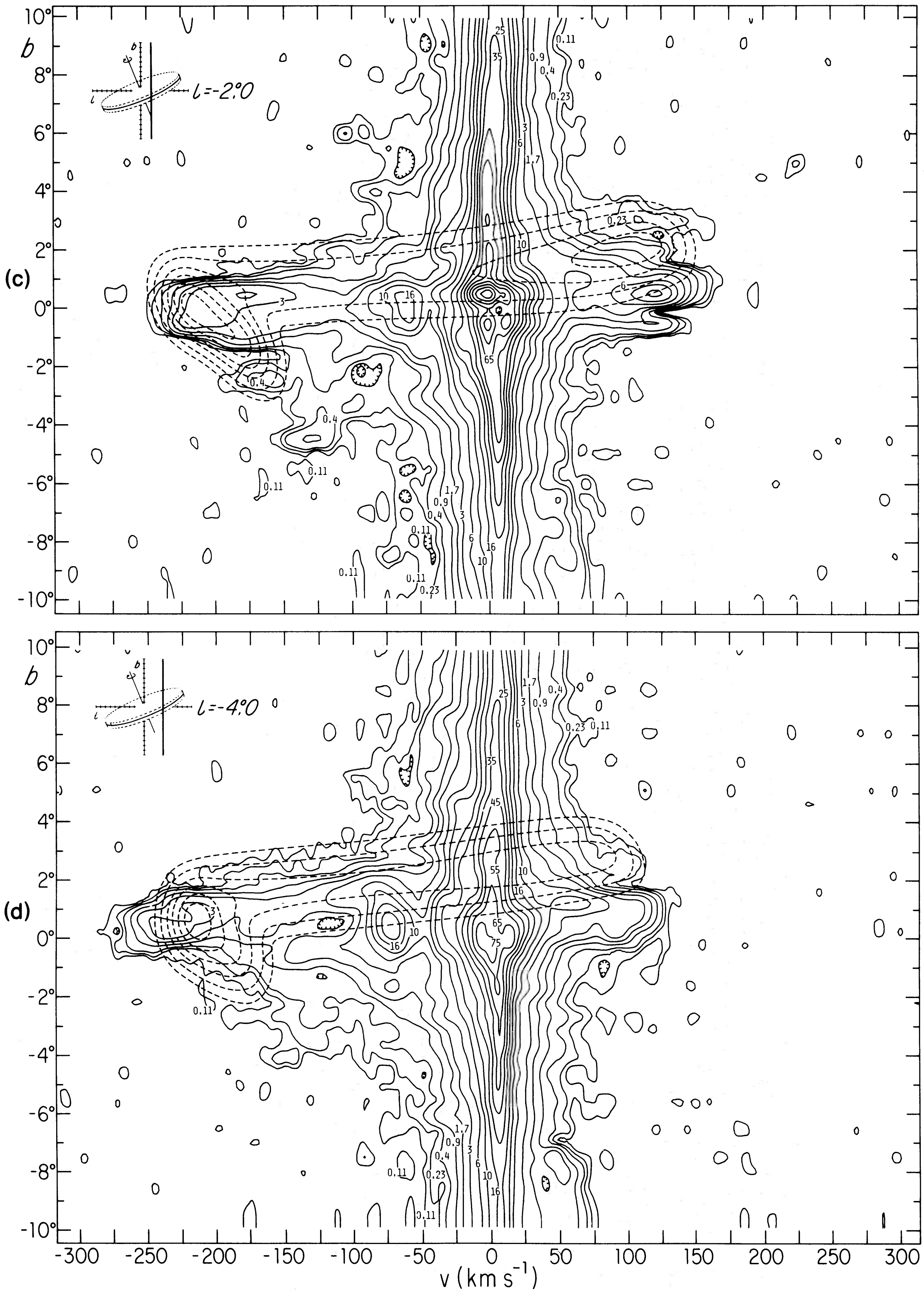
(c)
b
l=-2°.0
(d)
b
l=-4°.0
10°
8°
6°
4°
2°
0°
-2°
-4°
-6°
-8°
-10°
-300 -250 -200 -150 -100 -50 0 50 100 150 200 250 300
v (km s^-1)

IX. SUMMARY: CONSTRAINTS ON GALACTIC-NUCLEUS DYNAMICS: SPECULATIONS ON GALACTIC CONSEQUENCES

The model of the inner-Galaxy gas distribution described here invokes rotation and outward flow of comparable magnitude in an inclined thin disk. The density of gas in the model varies only with distance from the mean plane of the disk. The velocity fields are axisymmetric and simply described. Within this disk, we see no compelling evidence of important density enhancements or kinematic perturbations associated with particular observational features. We also see no evidence of recurring anisotropic ejections of material from the galactic nucleus. The smooth variation and complete axial symmetry shared by all parameters of our synthesis imply that a steady state prevails. Although our phenomenological analysis involves no dynamical underpinning, its usefulness in explaining apparently unrelated aspects of the observations does suggest that it can reasonably be used to constrain the dynamics of the inner-Galaxy material.

To summarize many of the discussions in the text, we catalog in Table 2 the specific observational features, previously studied separately and identified with bars, spiral arms, ejecta, etc., which are subsumed by our synthesis. The synthetic line profiles exhibit also the most important general trends in the data; as discussed above, these include coherent deviations of the emission centroids from complete symmetry about the planes $l = 0°$ or $b = 0°$. We repeat that the model parameters were not adjusted to account separately for individual observational features. Our explanation of the various inner-Galaxy phenomena renders moot some of the most troubling and unsatisfying aspects of earlier interpretations of material observed at both seemingly permitted and forbidden velocities. Thus the apparent asymmetries about the plane $l = 0°$ of the conventional "rotation nuclear disk" are explained, and its characteristic signature in the l, v plane is reproduced by a medium of essentially constant density in which expansion dominates the kinematics close to the galactic center. The "connecting arm" is another example of a prominent feature at "permitted" velocities which is accounted for without density enhancements. Confinement of all the observed emission from inner-Galaxy H I to $|v| < 280$ km s^{-1} (see Mirabel 1976; Burton, Gallagher, and McGrath 1977) has been puzzling in the context of the variety of proposed high-velocity ejections. Oort (1977) has stressed that when the only restraint on a test particle's motion is the usually adopted galactic gravitational field, an initial velocity of 740 km s^{-1} is necessary for the particle to reach $|z| = 500$ pc, corresponding to $|b| = 2\overset{\circ}{.}9$ (cf. Figs. 8*a*, 8*b*, 8*i*, and 8*j*). We see it as an advantage of the present model that it accounts for the similar velocity extents of both the apparently regular and anomalous-velocity material. It has also been puzzling that conditions near the galactic nucleus, which are clearly favorable to gas in a neutral state with high molecular abundance, have not been disrupted by the earlier proposed recurring violence. The equilibrium situation suggested by our model is more compatible with the observed gas qualities.

As it is presently constituted, the H I mass of the inclined disk is 1×10^7 $M_\odot$, and some 4 $M_\odot$ yr^{-1} of this material cross the disk boundary due to the Π_d motion. As will be shown in the next paper in this series, the kinematics of atomic and molecular hydrogen (as traced by carbon monoxide) are essentially identical, and the total mass of the gaseous disk is much increased. If a net outward flow exists, a gas input source or recirculation mechanism must ultimately be specified. Unless an extended source was present, conservation of mass and angular momentum would require that both n_d and Θ_d be proportional to ϖ_d^{-1} in uniformly expanding portions of the disk ($\varpi_d \gtrsim$ 0.2 kpc). Because we have been concerned here with demonstrating the existence of a varied but intrinsically coherent kinematic signature in the observations, we have not included a ϖ_d variation in n_d such as might arise from fitting modeled and observed intensities. Likewise, although our function Θ_d decreases at $\varpi_d > 0.85$ kpc, the model was not constructed in such a way as to constrain angular momentum. The dynamics of the disk remain to be specified, particularly as the required Θ_d motion cannot be related to the gravitational potential or total (stellar) mass in any direct fashion.

The galactic-scale consequences of the disk depend crucially on the total amount of material confined to the tilted inner-Galaxy plane. Indeed, the gravitational potential must have a form which will not cause rapid disruption of the disk by differential precession. A strong, spherically symmetric potential would preserve the disk structure as well as its orientation. Alternatively, concentration of a large stellar mass component to the inclined plane might result in a uniform precession of the entire assembly of gas and stars. Direct evidence relating to the alignment of the stellar system in the inner Galaxy is lacking. The distribution of infrared or thermal radio emission is dominated by the central concentration of molecular clouds and H II regions in the Sagittarius source complex.

FIG. 10*a*.—Emission in the b, v plane at $l = +4\overset{\circ}{.}0$. Encompassed by the synthesis are the features X and XII of van der Kruit (1970) and J4 of Cohen (1975).

FIG. 10*b*.—Emission in the b, v plane at $l = +2\overset{\circ}{.}0$. Figure E of Sanders *et al.* (1972) is the one observed and modeled at $b = -2\overset{\circ}{.}5$, $v \approx -125$ km s^{-1}.

FIG. 10*c*.—Emission in the b, v plane at $l = -2\overset{\circ}{.}0$. The positive-velocity portion of the model b, v distribution encompasses the feature pointed out by Sanders and Wrixon (1972*b*) and subsequently discussed by Cohen (1975) as J2. Also present is feature VII of van der Kruit (1970).

FIG. 10*d*.—Emission in the b, v plane at $l = -4\overset{\circ}{.}0$: This cut shows a relatively smooth distribution of emission. The model adequately accounts for the observed shift of the emission centroid to positive latitudes.

While we have not attempted to include the effects of a strong central mass concentration, the observations of carbon monoxide presented in the next paper in this series indicate that Sgr B2 partakes of the tilt of the inner-Galaxy gas despite its aberrant kinematics. Lacking kinematic information, observations of the continuum suffer from inability to discriminate between inner-Galaxy and transgalactic emission (arising over potentially as much as a $\sim$25 kpc path). The distribution of nonthermal radio emission shows a pronounced tilt in the inner 0.3 kpc (Kerr and Sinclair 1966) but is approximately symmetric about $b = 0°$ in the large-scale maps of Altenhoff *et al.* (1970).

The consequences for the entire Galaxy of a precessing out-of-plane mass distribution some 3 kpc in diameter would be far-reaching if the mass were considerable and if the distribution survived. There would undoubtedly exist a variety of responses due to resonances with the several characteristic frequencies of the galactic material. We speculate that the observed corrugations of the mean galactic layer (e.g., Quiroga 1974; Lockman 1977) might be related to the existence of an oscillating inner-Galaxy potential, as might the observed warping and thickening of the outer galactic layers. In this regard, we note that NGC 5907 and several other galaxies studied by Sancisi (1976) exhibit such outer-region behavior in the absence of companions with which they might interact tidally. Finally, we speculate that the gravitational potential generated by the tilted disk might serve as a driving force for spiral density enhancements or that spiral arms might otherwise be evolving phenomena associated with it.

It is worth noting that nonalignment of rotation axes seems to exist on a wide range of scales in other galaxies. On the smallest scale (a few parsecs) Light, Danielson, and Schwarzschild (1974) found that the core of M31 shows a flattened nucleus which is tilted relative to the major axis of the main system. They concluded that the nucleus of M31 is a distinct structure, dynamically separate from the rest of the galaxy (see also Johnson 1961). Rubin, Thonnard, and Ford (1977) report that the rotation axis of the excited nuclear gas in the inner $\sim$0.4 kpc of NGC 3672 makes a large angle with respect to the rotation axis of the galaxy as a whole. On a large scale, we recall the large angles which commonly separate the axes of radio galaxies from the rotation axes of their parent ellipticals.

The general dynamical relationship of galactic nuclei to entire galactic systems constitutes an important problem whose understanding can be advanced by the wealth of detail available in our own Galaxy. We are currently extending the sensitivity, extent, and density of the H I material with particular attention focused on the speculative polar-axis streams. The carbon monoxide observations reported in Paper II are also being extended, although, because the narrow beam available at short ratio wavelengths makes complete coverage impossible, we are searching for specific aspects of the expected disk signature. It may also be possible to take an alternative view of the present model which eliminates the mass flux and large kinetic energy implied by the presence of a net outward flow. The present model delineates fairly clearly the Θ_d and Π_d motions which will reproduce the perceived velocity fields. If similar motions could be recovered in another manner the observations would be equally well reproduced. The tilted nature of the overall distribution would remain inescapable. We are attempting to model the inner-Galaxy kinematics using elliptical streamlines such as might represent a central barlike configuration. This procedure was used by Peters (1975) in an attempt to account for the "3 kpc arm" and "135 km s^{-1} expanding arm" features, but was suggested to us independently by J. P. Ostriker. The observational consequences of such a distribution will be the subject of a later paper in this series.

REFERENCES

Altenhoff, W. J., Downes, D., Goad, L., Maxwell, A., and Rinehart, R. 1970, *Astr. Ap. Suppl.*, **1**, 319.
Baker, P. L., and Burton, W. B. 1975, *Ap. J.*, **198**, 281.
Bania, T. M. 1977, *Ap. J.*, **216**, 381.
Burton, W. B. 1970, *Astr. Ap. Suppl.*, **2**, 261.
———. 1971, *Astr. Ap.*, **10**, 76.
———. 1972, *Astr. Ap.*, **19**, 51.
Burton, W. B., Gallagher, J. S., and McGrath, M. A. 1977, *Astr. Ap. Suppl.*, **29**, 123.
Burton, W. B., and Gordon, M. A. 1978, *Astr. Ap.*, **63**, 7.
Cohen, R. J. 1975, *M.N.R.A.S.*, **171**, 659.
———. 1977, *M.N.R.A.S.*, **178**, 547.
Cohen, R. J., and Davies, R. D. 1976, *M.N.R.A.S.*, **175**, 1.
Cugnon, P. 1968, *Bull. Astr. Inst. Netherlands*, **19**, 363.
d'Odorico, S., Sancisi, R., and Simonson, S. C., III. 1969, *Astr. Ap.*, **1**, 131.
Hulsbosch, A. N. M. 1968, *Bull. Astr. Inst. Netherlands*, **20**, 33.
Johnson, H. M. 1961, *Ap. J.*, **133**, 309.
Kerr, F. J. 1967, in *Radio Astronomy and the Galactic System*, ed. H. van Woerden (London: Academic Press), p. 239.
Kerr, F. J., and Sinclair, M. W. 1966, *Nature*, **212**, 166.
Light, E. S., Danielson, R. E., and Schwarzschild, M. 1974, *Ap. J.*, **194**, 257.
Lindblad, P. O. 1974, *Astr. Ap. Suppl.*, **16**, 207.
Lockman, F. J. 1977, *A.J.*, **82**, 408.
Mirabel, I. F. 1976, *Ap. Space Sci.*, **39**, 415.
Mirabel, I. F., Pöppel, W. G. L., and Vieira, E. R. 1975, *Ap. Space Sci.*, **33**, 23.
Mirabel, I. F., and Turner, K. C. 1975, *Ap. Space Sci.*, **38**, 381.
Oort, J. H. 1968, in *IAU Symposium 29, Nonstable Phenomena in Galaxies*, ed. M. Arakeljan (Yerevan: Armenian Acad. Sci.), p. 41.
———. 1977, *Ann. Rev. Astr. Ap.*, **15**, 295.
Peters, W. L. 1975, *Ap. J.*, **195**, 617.
Quiroga, R. 1974, *Ap. Space Sci.*, **27**, 323.
Rougoor, G. W. 1964, *Bull. Astr. Inst. Netherlands*, **17**, 381.
Rougoor, G. W., and Oort, J. H. 1960, *Proc. Nat. Acad. Sci.*, **46**, 1.
Rubin, V. C., Thonnard, N., and Ford, W. K., Jr. 1977, *Ap. J.* (*Letters*), **217**, L1.
Sancisi, R. 1976, *Astr. Ap.*, **53**, 159.
Sanders, R. H., and Lowinger, T. 1972, *A.J.*, **77**, 292.
Sanders, R. H., and Wrixon, G. T. 1972*a*, *Astr. Ap.*, **18**, 92.
———. 1972*b*, *Astr. Ap.*, **18**, 467.
———. 1973, *Astr. Ap.*, **26**, 365.

1978ApJ...225..815B

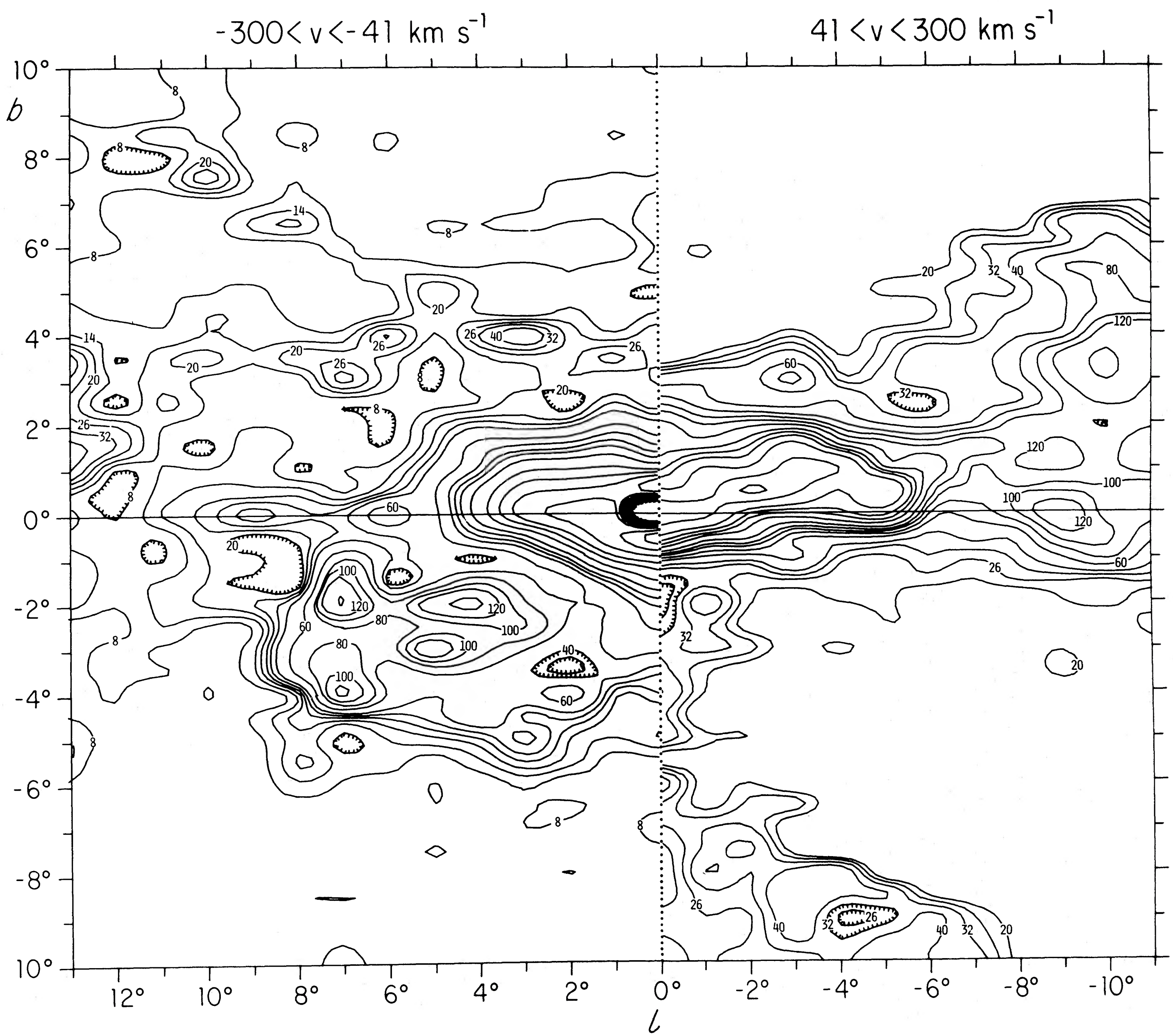

FIG. 11.—Contours of observed antenna temperature integrated over the velocity ranges $-300 < v < -41$ km s^{-1} (*left*) and $+41 < v < +300$ km s^{-1} (*right*). The choice of the velocity intervals excludes most of the emission from the Galaxy at large. The negative-velocity stream running from $b = 3°$, $l = 0°$, where it blends on the plane of the sky with the inner-Galaxy disk material, to $b = 10°$, $l = 13°$, where it leaves the observed space. At positive velocities the south polar axis stream runs from $b = -4°$, $l = 2°$, where it blends on the plane of the sky with the inner-Galaxy disk material, to $b = -10°$, $l = -6°$, where it leaves the observed space. Mirabel and Turner (1975) follow the feature to $b = -22°$, $l = -10°$.

Sanders, R. H., Wrixon, G. T., and Mebold, U. 1977, *Astr. Ap.*, **61**, 329.
Sanders, R. H., Wrixon, G. T., and Penzias, A. A. 1972, *Astr. Ap.*, **16**, 322.
Sandqvist, Aa. 1974, *Astr. Ap.*, **33**, 413.
Saraber, M. J. M., and Shane, W. W. 1974, *Astr. Ap.*, **36**, 365.
van der Kruit, P. C. 1970, *Astr. Ap.*, **4**, 462.
———. 1971, *Astr. Ap.*, **13**, 405.

W. B. Burton: Department of Astronomy, University of Minnesota, 116 Church Street, SE, Minneapolis, MN 55455

H. S. Liszt: National Radio Astronomy Observatory, Edgemont Road, Charlottesville, VA 22901